



## Postglacial sedimentary processes on the Storfjorden and Kveithola trough mouth fans: Significance of extreme glacial marine sedimentation



R.G. Lucchi<sup>a,b,\*</sup>, A. Camerlenghi<sup>a,b,c</sup>, M. Rebesco<sup>a</sup>, E. Colmenero-Hidalgo<sup>d,e</sup>, F.J. Sierro<sup>d</sup>, L. Sagnotti<sup>f</sup>, R. Urgeles<sup>g</sup>, R. Melis<sup>h</sup>, C. Morigi<sup>i</sup>, M.-A. Bårçena<sup>d</sup>, G. Giorgetti<sup>j</sup>, G. Villa<sup>k</sup>, D. Persico<sup>k</sup>, J.-A. Flores<sup>d</sup>, A.S. Rigual-Hernández<sup>d</sup>, M.T. Pedrosa<sup>b</sup>, P. Macri<sup>f</sup>, A. Caburlotto<sup>a</sup>

<sup>a</sup> OGS (Istituto Nazionale di Oceanografia e di Geofisica Sperimentale), Borgo Grotta Gigante 42/c, I-34010 Sgonico, Trieste, Italy

<sup>b</sup> Departament d'Estratigrafia, Paleontologia i Geociències Marines, Universitat de Barcelona, Facultat de Geologia, C/Martí i Franquès, s/n, E-08028 Barcelona, Spain

<sup>c</sup> ICREA, Institució Catalana de Recerca i Estudis Avançats, E-08028 Barcelona, Spain

<sup>d</sup> Department of Geology, Faculty of Sciences, University of Salamanca, E-37008 Salamanca, Spain

<sup>e</sup> Facultad de CC. Biológicas y Ambientales, Universidad de León, Campus de Vegazana, s/n, E-24071 León, Spain

<sup>f</sup> Istituto Nazionale di Geofisica e Vulcanologia, Via di Vigna Murata 605, I-00143 Roma, Italy

<sup>g</sup> Institut de Ciències del Mar (CSIC), Passeig Marítim de la Barceloneta, 37-49, E-08003 Barcelona, Spain

<sup>h</sup> Dipartimento di Geoscienze, Università di Trieste, Via E. Weiss 2, I-34128 Trieste, Italy

<sup>i</sup> Department of Stratigraphy, Geological Survey of Denmark and Greenland (GEUS), Øster Voldgade 10, DK-1350 Copenhagen K, Denmark

<sup>j</sup> Dipartimento di Scienze della Terra, Università di Siena, via Laterina 8, I-53100 Siena, Italy

<sup>k</sup> Dipartimento di Fisica e Scienze della Terra "Macedonio Melloni", Parco Area delle Scienze, 157A, 43124 Parma, Italy

### ARTICLE INFO

#### Article history:

Received 29 October 2012

Received in revised form 4 October 2013

Accepted 17 October 2013

Available online 29 October 2013

#### Keywords:

Barents Sea  
sedimentary processes  
LGM  
meltwater plumes  
gullies  
MWP-1a

### ABSTRACT

The depositional history of the Storfjorden and Kveithola trough-mouth fans (TMFs) in the northwestern Barents Sea has been investigated within two coordinated Spanish and Italian projects in the framework of the International Polar Year (IPY) Activity 367, NICE STREAMS. The investigation has been conducted using a multidisciplinary approach to the study of sediment cores positioned on high-resolution multibeam bathymetry and TOPAS/CHIRP sub-bottom profiles.

Core correlation and the age model were based on 27 AMS <sup>14</sup>C samples, rock magnetic parameters, lithofacies sequences, and the presence of marker beds including two oxidized layers marking the post Last Glacial Maximum (LGM) inception of deglaciation (OX-2) and the Younger Dryas cold climatic event (OX-1).

Sediment facies analysis allowed the distinction of a number of depositional processes whose onset appears closely related to ice stream dynamics and oceanographic patterns in response to climate change. The glacial diamicton with low water content, high density, and high shear strength, deposited during glacial maxima, indicates ice streams grounded at the shelf edge. Massive release of IRD occurred at the inception of deglaciation in response to increased calving rates with possible outer ice streams lift off and collapse. The presence of a several-meter-thick sequence of interlaminated sediments deposited by subglacial outbursts of turbid meltwater (*plumites*) indicates rapid ice streams' melting and retreat. Crudely-layered and heavily-bioturbated sediments were deposited by contour currents under climatic/environmental conditions favorable to bioproductivity.

The extreme sedimentation rate of 3.4 cm a<sup>-1</sup> calculated for the plumites from the upper-slope area indicates a massive, nearly instantaneous (less than 150 years), terrigenous input corresponding to an outstanding meltwater event. We propose these interlaminated sediments to represent the high-latitude marine record of Meltwater Pulse 1a (MWP-1a). Different bathymetric and oceanographic conditions controlled locally the mode of glacial retreat, resulting in different thickness of plumites on the upper continental slope of the Storfjorden and Kveithola TMFs. It is possible that the southern part of Storfjorden TMF received additional sediments from the deglaciation of the neighboring Kveithola ice stream.

© 2013 The Authors. Published by Elsevier B.V. Open access under [CC BY-NC-ND license](http://creativecommons.org/licenses/by-nc-nd/3.0/).

### 1. Introduction

Trough-mouth fans (TMF) are sedimentary depocenters located at the mouth of cross-shelf glacial troughs on continental shelves (Vorren and Laberg, 1997; Taylor et al., 2002). TMFs represent the major sites of terrigenous sediment accumulation originating from ice streams within former ice sheets on high-latitude continental margins. Understanding

\* Corresponding author at: OGS (Istituto Nazionale di Oceanografia e di Geofisica Sperimentale), Borgo Grotta Gigante 42/c, I-34010 Sgonico, Trieste, Italy. Tel.: +39 040 2140355; fax: +39 040 327307.

E-mail address: [rglucchi@ogs.trieste.it](mailto:rglucchi@ogs.trieste.it) (R.G. Lucchi).

TMF sedimentation is therefore important in order to reconstruct the recent glacial history of the planet, to understand past ice sheet dynamics from the marine sedimentary record, and to decipher paleoclimate and paleoenvironments during key periods, such as glacial maxima and the transitions to warm interglacial periods (deglaciation).

TMFs are equivalent in size, volume, and sediment mass to deep-sea fans originating from large river-fed sedimentary systems located on mid- to low-latitude continental margins. While the mechanisms of sediment transfer and deposition of deep-sea fans are well known, and have been summarized in detailed sedimentary models driven by turbidity currents (e.g., Shanmugam, 2000), such comprehensive sedimentary models still lack for TMFs. The initial conceptual model of TMF as a rather uniform sedimentary system dominated by glacial–interglacial rhythmic sedimentation (e.g., Alley et al., 1989; Vorren et al., 1989, 1998; Vorren and Laberg, 1997) is being revised due to the evidences of complexity of subglacial and pro-glacial environment processes (e.g., Ó Cofaigh et al., 2003; Laberg et al., 2005; Shaw et al., 2006; Dowdeswell et al., 2008; Piper et al., 2012).

This study aims to describe the mechanisms of sediment transport and dispersion on the continental slope of TMFs during the deglaciation that followed the LGM in response to climate change and glacial dynamics. The study area is appropriate for this detailed sedimentological study because of the relatively small catchment area of the Storfjorden glacial system, the relatively short residence time of ice in the ice stream, and the location of the glacial sedimentary system close to the interaction between Atlantic and Arctic water masses. We specifically report on the role of subglacial meltwaters in the sedimentary patterns of high-latitude continental slopes facing TMFs as it results from lateral and temporal variability of the grounding line retreat during deglaciation.

This study derives from an international, multi-disciplinary effort carried out within a combined investigation resulting in two coordinated cruises: the SVAIS cruise on board the BIO Hespérides (summer 2007) and the OGS-EGLACOM cruise on board the R/V OGS-Explora (summer 2008). SVAIS and OGS-EGLACOM projects share objectives within the International Polar Year (IPY) Activity 367 NICE STREAMS (Neogene Ice Streams and Sedimentary Processes on High-Latitude Continental Margins).

## 2. Study area

### 2.1. Inferred paleo-ice drainage

Previous studies (Ottesen et al., 2006; Andreassen et al., 2008; Pedrosa et al., 2011) reported that the glacial drainage area that fed the Storfjorden TMF (Fig. 1) extends to the continental divide of Spitsbergen and Edgeøya islands (of Svalbard), Hopen Island, Bjørnøya, and the submerged divide along Spitsbergenbanken separating these islands. The resulting drainage area is approximately 82,500 km<sup>2</sup>, which is small relatively to the main glacial drainage systems of the Barents and Kara Sea, such as Byørnøyrenna, Franz Victoria Trough, Svyataya Anna Trough, and Voronin Trough (Svendsen et al., 2004; Murdmaa et al., 2006). Nothing is known on past changes in ice flow source and direction as identified in other paleo-ice streams in the area (Dowdeswell et al., 2010; Sarkar et al., 2011).

### 2.2. Water masses

The Western Barents Sea and the West Spitsbergen continental margins form the physical boundary of the northward flowing Norwegian

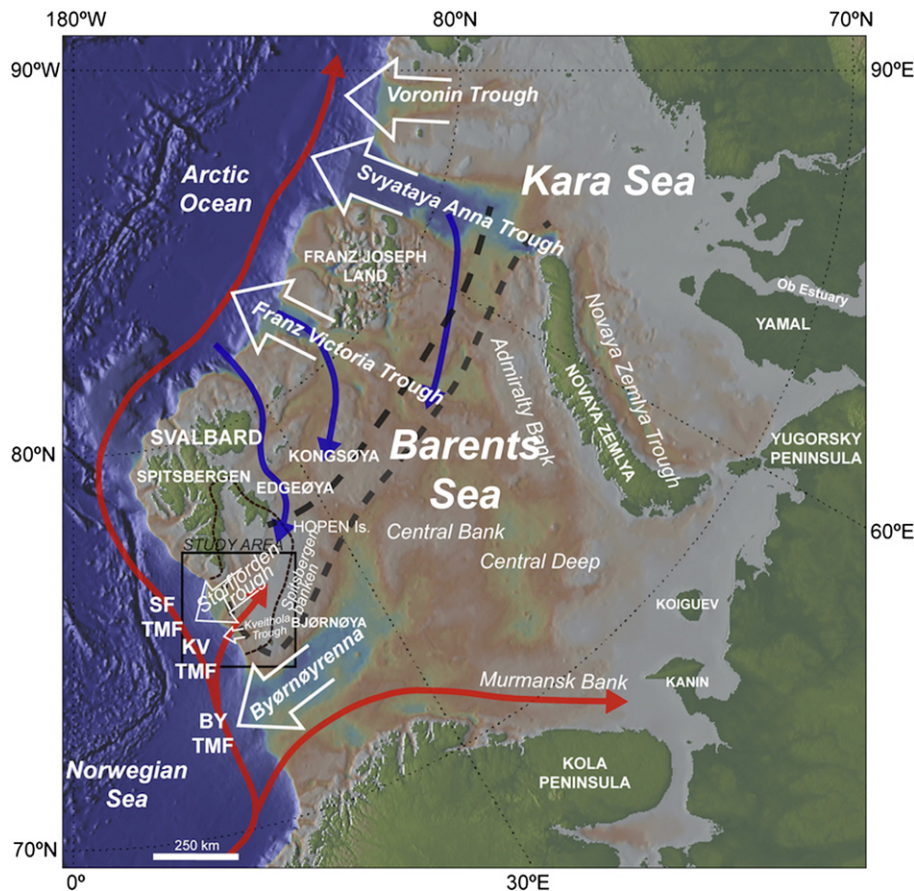


**Fig. 1.** Map of the North-western Barents Sea indicating the main ice streams pathways during the last glacial stage (white arrows), and the heat conveyor belt pattern in the North Atlantic area (red arrows indicate warm currents; blue arrows cold currents; see text for explanation of currents and fronts names). The black box indicates the study area. BY = Byørnøyrenna; SF = Storfjorden; KV = Kveithola; TMF = Trough Mouth Fan.

Atlantic Current (NwAC) and West Spitsbergen Current (WSC), derived from the North Atlantic Current (Slubowska-Woldengen et al., 2008) (Fig. 1). A branch of the WSC enters the Storfjorden Trough where it meets the southward flowing East Spitsbergen Current (ESC), forming two water mass fronts: the Polar Front (PF), to the north, and the Arctic Front (AF), to the south, both variably located on the continental shelf of the Storfjorden Trough.

An oceanographic characteristic of the study area is the presence of a stable polynya forming in Storfjorden s.s. during wintertime with associated formation of brine-enriched shelf water (BSW) (Skogseth et al., 2005). The topographic sill amid the fjord determines the accumulation of the dense brine in the rimmed fjord basin, and the periodic spillover towards the outer Storfjorden continental shelf, which represents one of the densest water masses in the Barents Sea (Geyer et al., 2009).

Kveithola Trough, located immediately to the south of Storfjorden Trough (Rebesco et al., 2011), from which it is topographically separated by Spitsbergenbanken, is also the site of production of continental shelf dense waters. These waters are a consequence of salt rejection during

sea-ice formation with generation of temperature-salinity dense plumes (TS plumes), often enriched in re-suspended sediments that periodically cascade along the slope (Fohrmann et al., 1998).

### 2.3. Cenozoic evolution

The Storfjorden TMF (Hjelstuen et al., 1996; Laberg and Vorren, 1996) is underlain by a post-Palaeocene (55 Ma–Present) sedimentary sequence that locally reaches a thickness of about 8 km. A basal post-rift terrigenous sedimentary sequence of Palaeocene to Late Pliocene age, up to 6 km in thickness, is overlaid by up to 3 km of glacially-driven sequence that has determined the rapid progradation and aggradation of the TMF. River discharge from an emerged area now partly submerged on the continental shelf controlled the sedimentation of the pre-Late Pliocene fan, forming a mixed turbidite–contourite system identified in seismic reflection data (Unit G0 of Hjelstuen et al., 1996). The gradual onset of the northern hemisphere glaciation and the progressive expansion of the Barents Sea Ice Sheet on the continental

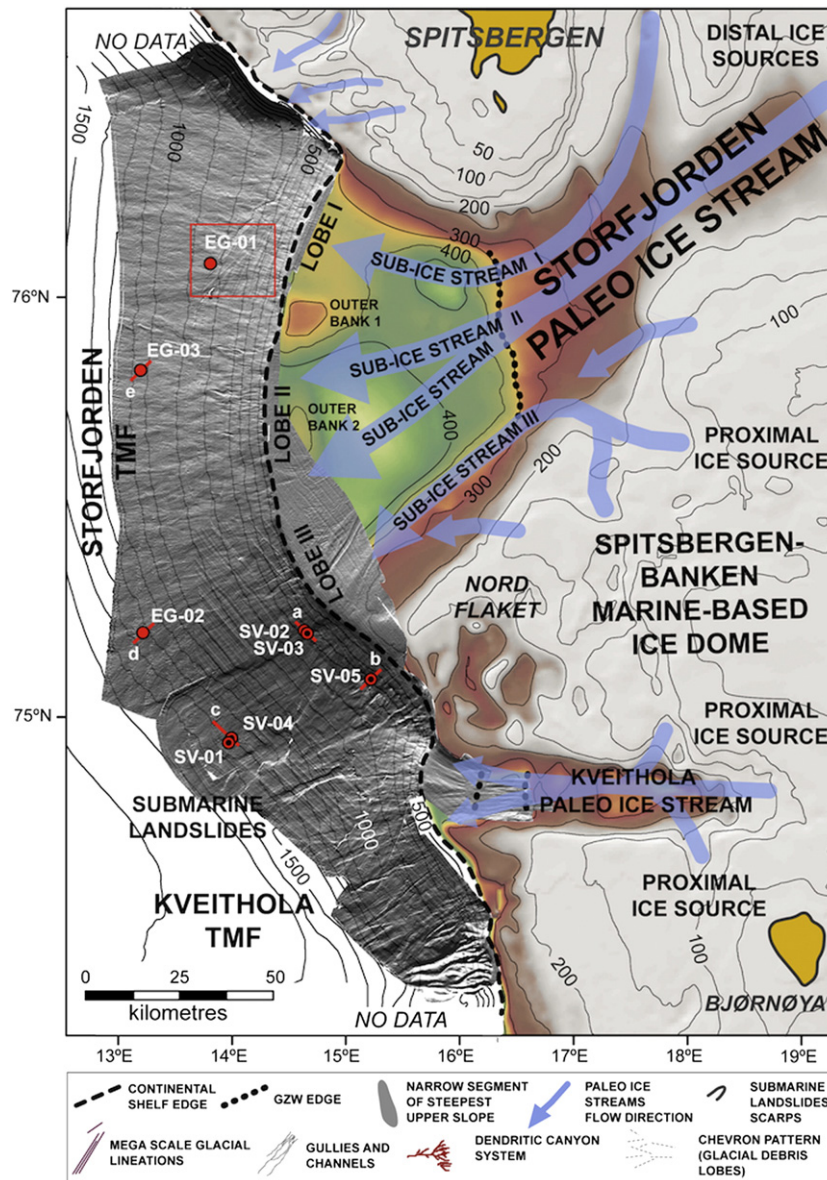


**Fig. 2.** Map of the study area with inferred direction of the main ice streams present during the LGM. SVAIS cores (SV-) are indicated with red-black circle, while EGLACOM cores (EG-) are indicated with red circles. Red segments indicate the location of the sub-bottom profiles associated to each core site (see Fig. 3). The red box locates the inset of Fig. 4B). The grey-scale shaded relief bathymetry derives from the merged high-resolution surveys carried out during the SVAIS and EGLACOM cruises (modified after Pedrosa et al., 2011). GZW = Grounding Zone Wedge.

shelf have determined the shift to the rapid accumulation of diamicton from glacially driven debris flows alternated with interglacial glacial marine sedimentation (Laberg and Vorren, 1996). The debris flow accumulation during glacial maxima was estimated as high as  $170 \text{ cm ka}^{-1}$ , while the contribution of the interglacial glacial marine sedimentation to the construction of the margin was considered nearly negligible (Laberg and Vorren, 1996). The continental shelf within the Storfjorden Trough is thought to have remained exposed subaerially, and therefore subject to very intense glacial erosion until about 1.4–0.8 Ma. Approximately 950 m of the total 1100 m of the sediment cover were eroded and removed from 2.3 to 0.8 Ma (Butt et al., 2002).

#### 2.4. Last glacial depositional architecture

High-resolution bathymetric and shallow seismic reflection records of Storfjorden TMF show three depositional lobes (Pedrosa et al., 2011). The two northernmost sedimentary lobes (Lobes I and II) (Fig. 2) are separated by an outer shelf bank, and are characterized by over 50 m of glacial debris flow deposits accumulated during the Weichselian glacial maxima (acoustic Unit B) (Fig. 3). On the upper slope, these deposits are incised by a dendritic pattern of gullies draped by a thin (2–3 m thick) interval of de-glacial and Holocene sediments (Unit A) (Fig. 3). On the modern seafloor, the gullies disappear at mid-slope, being replaced by a subdued chevron-like morphology inherited by the LGM glacial debris lobes buried by the uppermost thin sedimentary drape.

The southernmost Storfjorden Lobe III and the adjacent Kveithola TMF are characterized by several submarine landslides with headwalls located on the middle and upper slope, and stacked mass transport deposits (MTD) in the middle and lower slope subsurface (Rebesco et al., 2011, 2012; Lucchi et al., 2012) (Fig. 2). The disruption of the original depositional surface by gravitational instability of the continental slope hinders the recognition of the original seafloor morphology in this part of the margin. One of the major characteristics of the LGM depositional architecture of Lobe III is that the glacial debris flow deposits are either missing or are reduced to laterally discontinuous thin lenses (Pedrosa et al., 2011) (Fig. 3). Conversely, the interglacial sediments are composed of thick and laterally continuous acoustically laminated patterns (Units A1–A2) up to about 15 m thick.

Aside from the TMFs, the so-called inter-TMF areas of the continental slope display dendritic sediment drainage systems comprising canyons converging in deep-sea channels, such as the INBIS channel to the south of the study area (Laberg and Vorren, 2000; Laberg et al., 2010), which are absent elsewhere on the TMFs.

The lateral changes in sedimentary processes on Storfjorden TMF, at least from the acoustic record of the last glacial cycle, have been attributed to the presence of different sub-ice streams in Storfjorden Trough with different dynamics both during the maximum expansion of the ice sheet and during the deglaciation (Pedrosa et al., 2011).

Previous studies on the sediment record from South Svalbard and the middle slope of Storfjorden Lobe I suggest that deposition of glacial debris flows in the area occurred around  $23,820 \pm 260 \text{ cal. a BP}$ , while the evidence for deglaciation begins around  $20,500 \pm 500 \text{ cal. a BP}$ , with ice

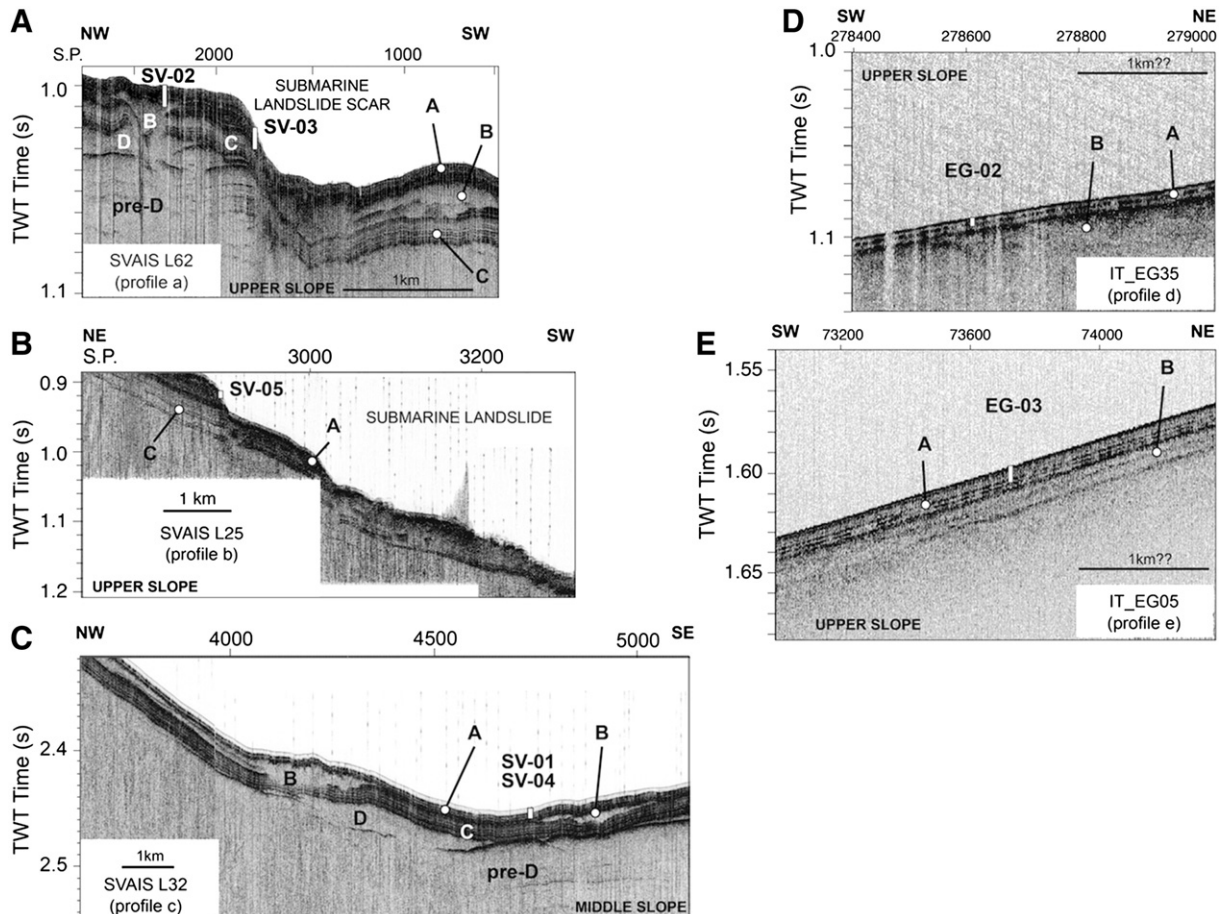


Fig. 3. Sub-bottom profiles indicating the acoustic stratigraphy at the core sites (Fig. 2). Acoustic Units A correspond to interglacial MIS-1; Unit B represents Late-Weichselian glacial stage MIS-2; and Unit C was associated with the Middle-Weichselian interglacial MIS-3 (see text for detail).

**Table 1**  
Core location.

Core ID	Lat N	Lon E	Water depth (m)	Location	Recovery (m)	N. of sections
SV-01	74°58.047'	13°55.550'	1813	Middle-slope lobe III	2.78	3
SV-02	75°13.707'	14°35.960'	743	Upper-slope lobe III	6.41	7
SV-03	75°13.352'	14°37.249'	761	Upper-slope lobe III	6.42	7
SV-03tc	75°13.352'	14°37.249'	762	Upper-slope lobe III	1.01	1
SV-04	74°57.425'	13°53.972'	1839	Middle-slope lobe III	3.03	4
SV-05	75°06.703'	15°13.307'	713	Upper-slope lobe III	6.32	7
EG-01	76°06.201'	13°37.625'	1069	Gully uppr slope lobe II	2.20	3
EG-02	75°12.907'	13°04.587'	1722	Middle-slope lobe III	3.05	2
EG-03	75°50.615'	12°58.353'	1432	Middle-slope lobe II	2.91	2

SV = SVAIS; EG = EGLACOM; tc = trigger core.

rafted debris present in the sediments until ca 10,100 cal. a BP (Jessen et al., 2010).

### 3. Materials and methods

This study focuses on nine sediment cores collected from the Storfjorden and Kveithola continental slopes, and sub-bottom profiles collected for core positioning and identification of shallow depositional structures (Table 1; Fig. 3). Details on the bathymetric and shallow seismic surveys are reported in Pedrosa et al. (2011).

Sediment cores were analyzed using both automated core-logging techniques with sampling measurements at 1 cm to 1 mm resolution, and traditional analytical methods on over 1000 discrete samples.

Core-scanning included: CAT-scan radiographs performed prior to core opening; high-resolution digital photos, color scan and chemical composition of the sediments by means of an Avaatech Superslit X-ray fluorescence core-scan (XRF-core scan) using 10 and 50 kV instrumental settings; sediments physical properties using a multi-sensor core logger for wet bulk density and magnetic susceptibility; and paleomagnetic/rock magnetic parameters performed on u-channels collected along the central part of the split sections.

Undrained shear strength analyses were performed on the undisturbed SVAIS cores every 10 cm using a British fall cone (Leroueil and Le Bihan, 1996).

Discrete sediment samples were collected at 10–5 cm resolution and analyzed for sediment physical properties and composition. Sediment water content was determined by oven-drying the sediments at 105 °C for 24 h. Grain size analyses were performed with a coulter-counter laser Beckman LS-230 to measure the 0.04–2000 µm fraction at 0.004 µm resolution. The samples were initially treated with diluted peroxide and the disaggregated sediments were re-suspended into a 0.1% sodium-hexametaphosphate solution and left for 3 min in ultrasonic bath prior to measurement. The results were classified according to Friedman and Sanders (1978) grain-size scale and were analyzed with the cluster statistical method.

The sand fraction mineralogy was determined through optical microscope and Scanning Electron Microscope (SEM) coupled with Energy Dispersive Spectroscopy (EDAX), while the mud fraction was investigated through smear-slides (after Rothwell, 1988).

Total and organic carbon ( $C_{tot}$ ,  $C_{org}$ ) and nitrogen ( $N_{tot}$ ) were measured on the cores SV-02 and SV-04 using a NA-2100 Elemental Analyser, following the procedure of Nieuwenhuize et al. (1994). Calcium carbonate ( $CaCO_3$ ) and organic matter (OM) contents were calculated following Gordon (1970). The distribution of marine and

**Table 2**  
Radiocarbon dating.

Sample ID	Lab ref.	Sample type	Description	Proceas	AMS <sup>14</sup> C	Age err.	δ13C	Cal. yr BP
<i>Upper slope</i>								
SV2-5-39/40	OS-77655	Foraminifera	Benthic + planktonic	HY	15,050	50	−0.24	17,748 ± 139
SV3-1-0/1	OS-77656	Foraminifera	Benthic + planktonic	HY	4860	30	−0.07	5039 ± 87
SV3-1-32/33	OS-82683	Mollusc	Bivalve	HY	13,000	45	1.09	14,929 ± 141
SV3-6-21/30	OS-82684	Forams & Ostracods	Benthic + plankt. + ostrac.	HY	13,200	50	−0.85	15,061 ± 146
SV3-6-52/53	OS-77680	Foraminifera	Benthic + planktonic	HY	13,300	50	−0.4	15,156 ± 117
SV3tc-1-18/19	OS-77681	Foraminifera	Mixed planktonic	HY	2880	30	−0.34	2543 ± 73
SV5-4-82/83	OS-82689	Foraminifera	Mix plankt. mostly Nps	HY	17,350	85	−0.08	20,055 ± 166
EG1-1-2.5/3.5	OS-78409	Sediment (Corg)	Powdered sediment	OC	4830	35	−22.38	4968 ± 78
EG1-2-23/24	OS-98259	Foraminifera	Benthic foraminifera	HY	12,500	110	−0.81	13,874 ± 121
EG1-2-64/65	OS-78452	Sediment (Corg)	Powdered sediment	OC	28,900	190	−24.47	32,792 ± 364
EG1-3-62/63	OS-78453	Sediment (Corg)	Powdered sediment	OC	36,700	310	−24.76	41,357 ± 273
<i>Middle slope</i>								
SV1-2-19/20	OS-77654	Foraminifera	Mixed planktonic	HY	7990	45	0.34	8368 ± 47
SV4-1-0/1	OS-77682	Foraminifera	Nps	HY	1100	25	0.44	594 ± 36
SV4-2-11/12	OS-77683	Foraminifera	Nps	HY	4000	30	0.83	3896 ± 56
SV4-2-48/49	OS-82685	Foraminifera	Mixed planktonic	HY	7110	30	0.5	7519 ± 38
SV4-2-59/60	OS-77684	Foraminifera	Nps	HY	7880	45	0.5	8264 ± 59
SV4-2-65/66	OS-77685	Foraminifera	Nps	HY	8180	35	0.33	8558 ± 58
SV4-2-85/86	OS-82686	Foraminifera	Mixed planktonic	HY	8690	30	−0.44	9292 ± 70
SV4-3-24/27	OS-82687	Foraminifera	Benthic + planktonic	HY	9790	30	0.64	10,558 ± 33
SV4-3-77/79	OS-82688	Foraminifera	Mixed planktonic	HY	12,050	40	0.09	13,389 ± 61
SV4-4-94/95	OS-77686	Foraminifera	Nps	HY	21,800	100	−0.07	25,438 ± 241
EG2-1-30/31	OS-78387	Foraminifera	Benthic + planktonic	HY	4570	130	−25	4665 ± 164
EG2-1-90/91	OS-78389	Foraminifera	Benthic + planktonic	HY	9460	180	0	10,235 ± 234
EG2-2-60/61	OS-78383	Forams & Pteropods	Benthic + plankt. + pterop.	HY	12,100	180	1.41	13,481 ± 181
EG3-1-90/91	OS-78385	Foraminifera	Benthic + planktonic	HY	4910	120	−25	5118 ± 161
EG3-2-56/57	OS-78382	Foraminifera	Benthic + planktonic	HY	8590	130	0.01	9147 ± 167
EG3-3-38/39	OS-78324	Foraminifera	Benthic + planktonic	HY	9740	80	0.73	10,508 ± 87

Nps = *Neogloboquadrina pachiderma* sx; OC = Organic Carbon; HY = Hydrolysis.

continental-derived organic matter was distinguished based on the  $C_{org}/N_{tot}$  ratio, according to Meyers (1994).

The clay mineral assemblage was determined through X-ray diffractograms (XRD) performed with an automated Philips PW1710 powder diffraction system, using  $CuK\alpha$  radiation (40 kV, 40 mA), following the sample preparation procedures described by Ehrmann et al. (1992) and Petschick et al. (1996). Each sample was analyzed between  $2^\circ$  and  $40^\circ 2\theta$ , with a step size of  $0.02^\circ 2\theta$ , in the air-dry state and after ethylene glycol solvation. Additionally, a slow scan, between  $23^\circ$  and  $25.5^\circ 2\theta$ , with a step size of  $0.005^\circ 2\theta$ , was performed to obtain a better resolution of the chlorite (004)–kaolinite (002) twin peaks. Diffractograms were processed using the MacDiff software (Petschick, University of Frankfurt, Germany) for semi-quantitative estimate of the main clay (i.e., smectite, illite, chlorite and kaolinite) mineral abundance using the weighting factors of Biscay (1965).

Micropaleontological analyses of diatoms, benthic and planktonic foraminifera, and calcareous nannofossils were performed for palaeo-environmental reconstructions and for the definition of the age model in support to the palaeomagnetic stratigraphy and radiocarbon dating.

Microfossil species identification and classification follow Loeblich and Tappan (1987), Wollenburg and Mackensen (1998), and Feyling-Hanssen et al. (1971) for benthic foraminifera; Hemleben et al. (1989) for planktonic foraminifera; Hine and Weaver (1998), Young (1998), S  ez et al. (2003), and Backman et al. (2009) for nannofossils; and Tomas (1997) for diatoms.

Selected rock magnetic parameters (i.e., magnetic susceptibility and anhysteretic remnant magnetization) were studied for the definition of the age model following the procedure described in Sagnotti et al. (2011), in which the radiometric ages from each core were transferred to a common stratigraphic depth using the basis of core SV-04, the core with highest number of calibrated  $^{14}C$  ages. The obtained age model was then refined for the Holocene interval by correlation of the tie-points to the closest stack curves of paleosecular variation and relative geomagnetic paleointensity.

Twenty-seven AMS  $^{14}C$  dating analyses were performed at selected stratigraphic intervals (Table 2). Age calibrations were performed with Calib 6.0 calibration software program (Stuiver and Reimer, 1993), using the marine09 calibration curve (Reimer et al., 2009), and applying

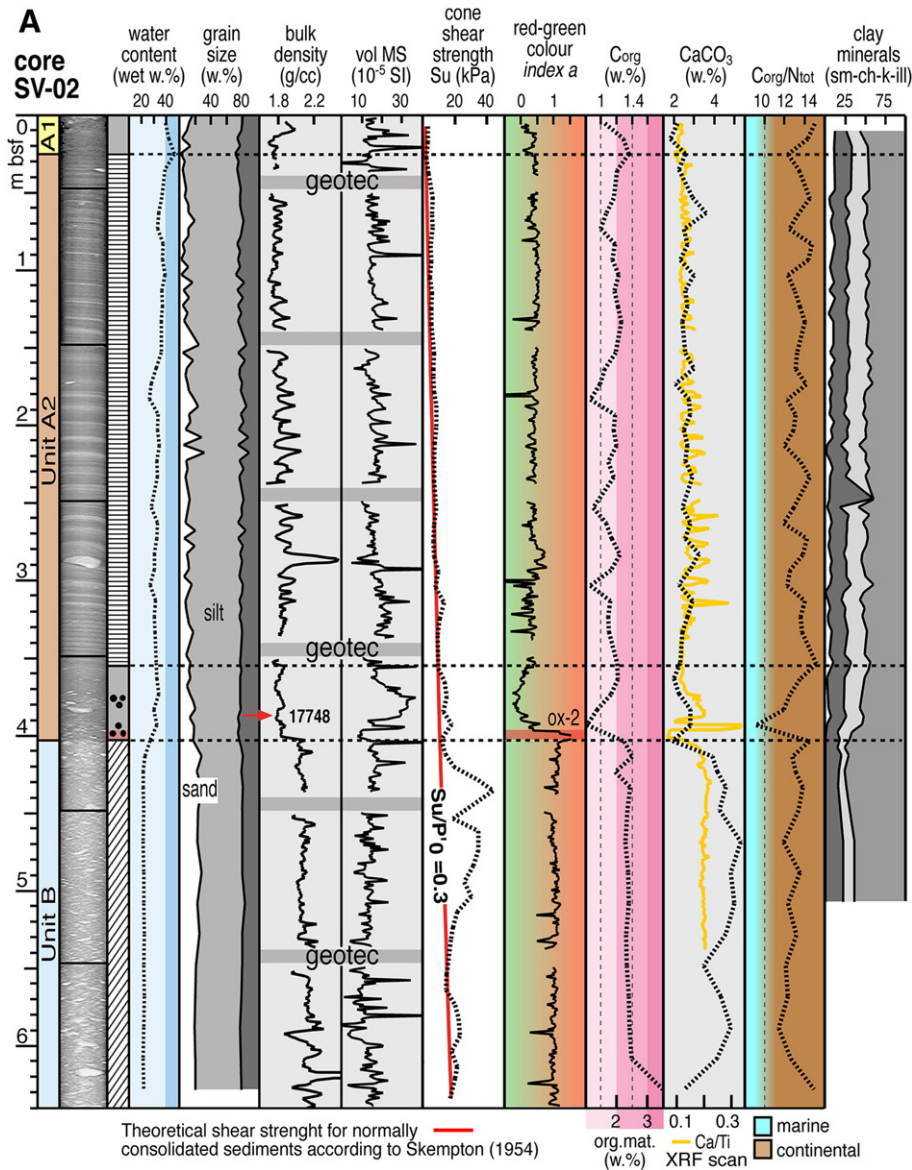


Fig. 4. A, B, C: Down-core logs of physical and compositional characteristics of the sediments. XRF data are indicated as ratio with the Ti detrital phase. Legend of lithofacies in C. The inset map in B was produced with the Hydrology analysis function of ArcGIS software interpreting the DTM in terms of water runoff in fluvial drainage system. The blue lines identify the resulting drainage pattern.

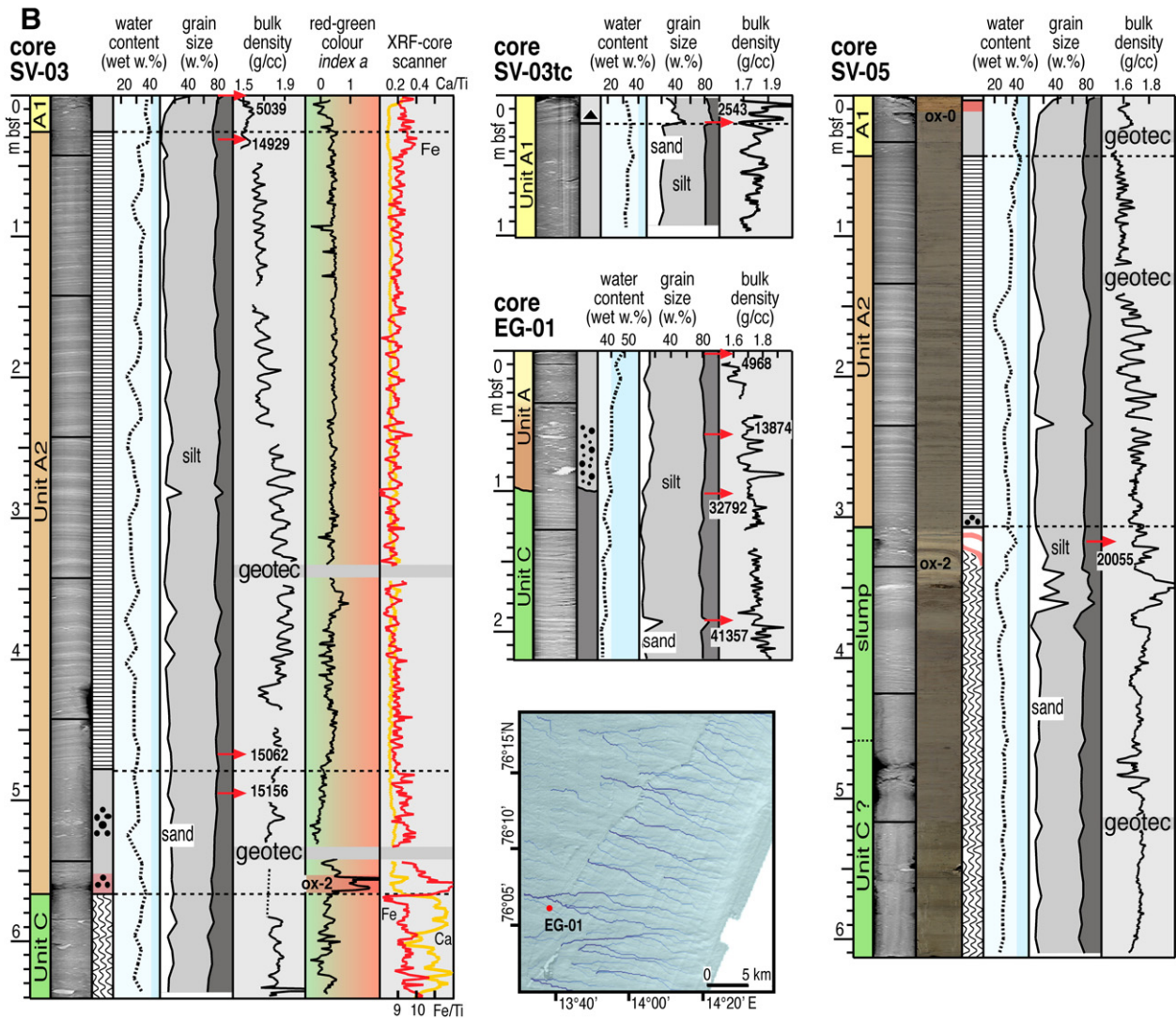


Fig. 4 (continued).

an average marine regional reservoir effect  $\Delta R = 84 \pm 23$  obtained from the Marine Reservoir Correction Database in Calib 6.0 for the northwestern Barents Sea area (south of Svalbard). The mean values from the calibrated age range of  $\pm 1\sigma$  were then normalized to calendar year (conventionally 1950 AD) and are in the following indicated as cal. a BP or as cal. ka BP.

#### 4. Results

##### 4.1. Sediment lithofacies and characteristics

Seven lithofacies were distinguished based on sediment visual description, radiograph facies, sediment physical properties, and composition.

##### 4.1.1. Stiff-massive diamicton (upper slope)

A stiff, very-dark grey diamicton was recovered at the base of core SV-02, located on the upper slope area (Fig. 4A). This lithofacies consists of a structureless/massive deposit containing abundant pebbles and gravel, randomly distributed in a firm, sticky sandy-mud matrix. The grain size distribution in the matrix is fairly constant, with 22% sand, 56% silt, and 22% clay proportions. This lithofacies is characterized by low water content (<20%), high wet bulk density (>2.1 g cm<sup>-3</sup>), high shear strength (up to 44 kPa), and very low MS (<10 SI<sup>-5</sup>). A comparison

between the measured undrained shear strength and the theoretical shear strength profile for normally consolidated sediments (Skempton, 1954), suggests strong consolidation of these sediments (Fig. 4A).

The composition of the sediments is fairly constant and consists of reworked foraminifera, abundant rounded quartz, and organic matter-rich black carbonate fragments often partially pyritized derived from subglacial erosion (Late Jurassic–Early Cretaceous Agardhfjellet Formation) (Sigmond, 1992). Fresh formed framboid crystals of pyrite are also present. In the down-core log, the presence of this lithofacies determines a sharp change of all parameters related to physical and compositional characteristics of the sediments. The lack of internal sedimentary structures and the fairly consistent texture of the sandy matrix suggest a process of transport and deposition “en masse,” with no grain size sorting.

##### 4.1.2. Slumped/reworked sediments (upper and middle slope)

Slumped/reworked sediments identified in the lower part of cores SV-05 and SV-04 determined sharp textural and compositional change in the stratigraphic sequence with irregular/sharp boundaries (Fig. 4B, C). In core SV-04, the presence of reworked sediments determines also a sharp drop of MS (Fig. 4C). Contrarily to the stiff-massive diamicton, slumped sediments are characterized by a higher water content (35% on average) and a lower bulk density (1.7 g cm<sup>-3</sup> on average).

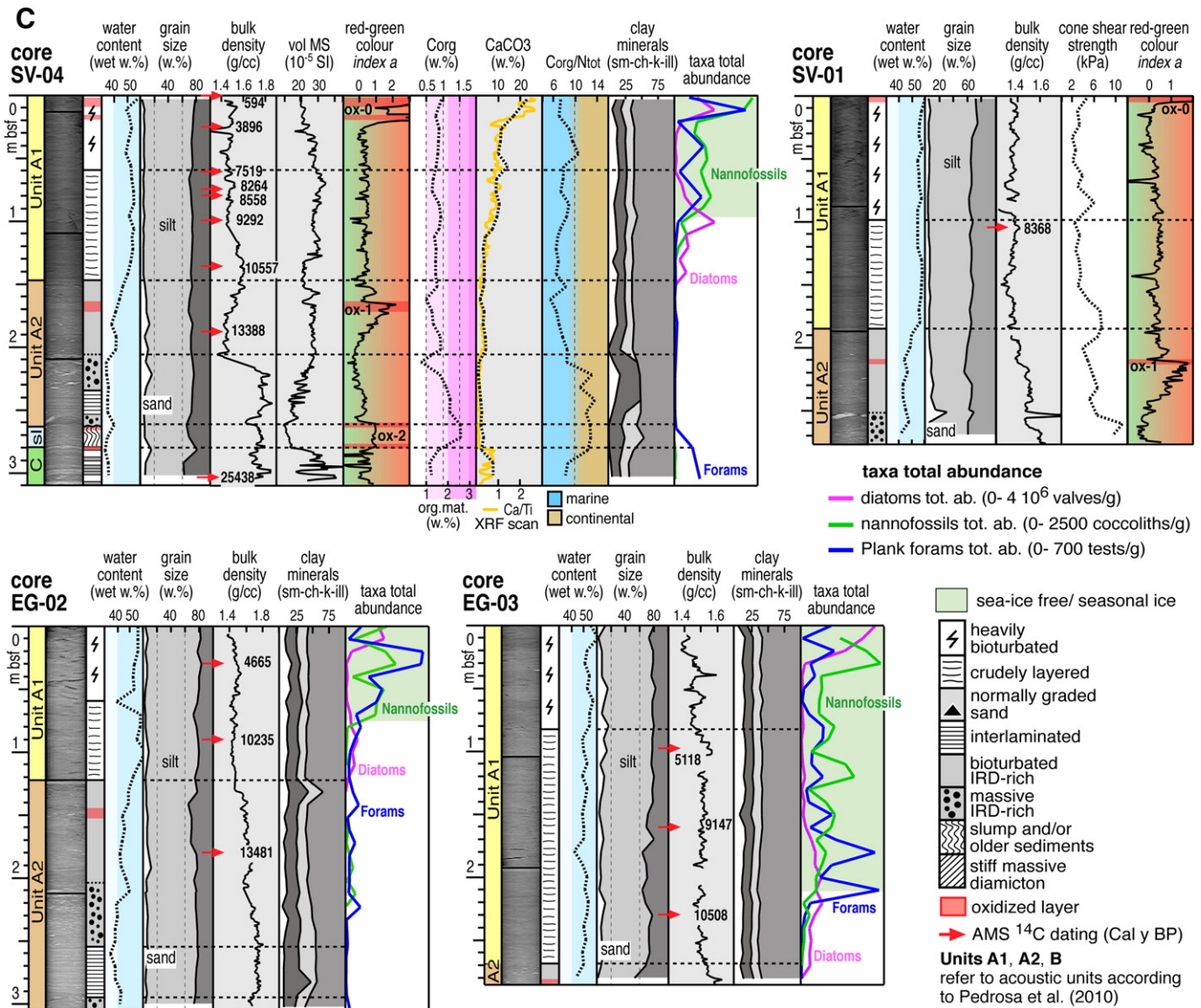


Fig. 4 (continued).

#### 4.1.3. IRD-rich sediments (upper and middle slope)

This facies is the most common along the entire sequence of both the upper and middle-slope areas, and is characterized by moderate to high density sediments, depending on the intensity of bioturbation and amounts of IRD (Fig. 4A, B, C). Two subfacies were distinguished: a structureless, coarse-massive subfacies formed by abundant large IRD pebbles, hereafter indicated as *coarse-massive-IRD facies*, and a finer-grained slightly bioturbated subfacies formed by gravel dispersed into a muddy matrix, hereafter indicated as *bioturbated-IRD-rich facies*.

The coarse-massive-IRD facies presents some radiographic similarities with the stiff-massive diamicton. However, the sediments are lighter in color, and are characterized by lower sediment bulk density ( $1.8 \text{ g cm}^{-3}$  on average), lower shear strength (20 kPa), higher water content (30%), and higher MS ( $15\text{--}30 \text{ SI}^{-5}$ ). The sediments are almost exclusively terrigenous with abundant quartz, orthoclase, Ca-plagioclase, and lithic fragments including the organic-rich black shale fragments. The bioclast component is very rare and usually reworked except for a small interval observed above oxidized layer OX-2 in core SV-02 (Ca peak, Fig. 5).

The bioturbated-IRD-rich facies is characterized by low bulk density ( $1.6 \text{ g cm}^{-3}$  on average), very low shear strength (6 kPa), and high

water content (40%). This subfacies is mainly terrigenous although it contains a larger fraction of bioclasts with respect to the coarse-massive-IRD facies.

#### 4.1.4. Interlaminated sediments (upper and middle slope)

This facies consists of almost barren, non-bioturbated, olive-grey sediments formed by finely laminated silty-clay sediments interbedded with centimeter- to millimeter-thick sand/silt layers (hereafter abbreviated as laminated mud and sandy layers respectively). The interlaminated sequence can contain IRD pebbles and cobbles (up to 8 cm across in core SV-02, Fig. 4A) and layered IRD (Figs. 4A, B, C).

The sandy layers are characterized by lower water content and higher sediment density and MS values compared to the laminated mud. Peaks of K, Si, and Ca content in the sandy layers correspond to abundant quartz, orthoclase, and Ca-plagioclase, while higher Fe content in the laminated mud relates to higher clay minerals content (Fig. 5). Rare glauconite was observed in the sandy layers, suggesting shelf provenance of the sediments. A comparison between the measured undrained shear strength and theoretical shear strength profile for normally consolidated sediments indicates normal consolidation of the sediments (Fig. 4A).

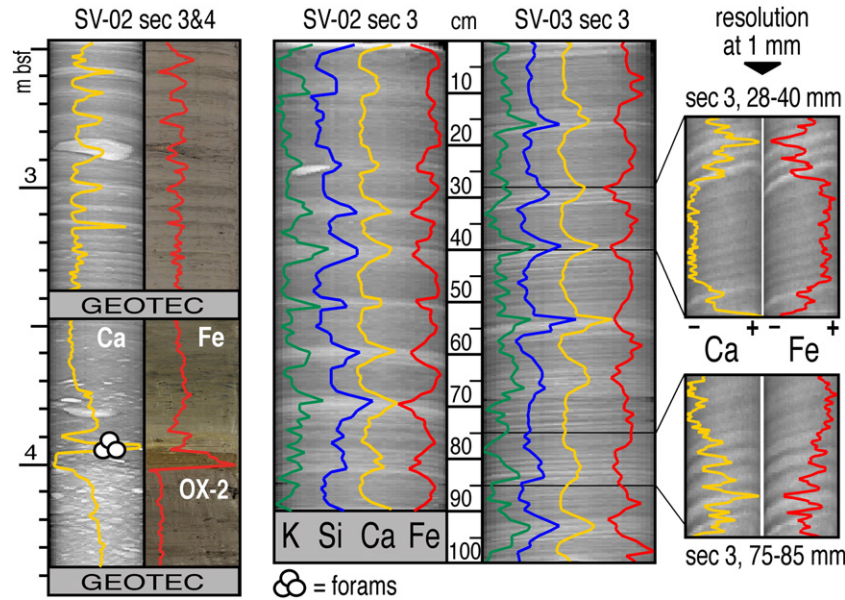


**Fig. 5.** Compositional characteristics of the coarse-massive-IRD and interlaminated facies determined through XRF core scan at 1 cm and 1 mm resolution. In the oxidized layer OX-2 of core SV-02 the Ca-peak corresponds to a foraminifera-rich horizon. The sandy layers of the interlaminated facies are pinpoint by peaks of K, Si, and Ca, (presence of K-feldspars, quartz and Ca-plagioclase), while high Fe characterize the laminated mud (clay minerals).

The grain size trend is characterized by a progressive fining-up sequence. This trend also corresponds to a decrease of the sandy layers thickness and occurrence within the interlaminated facies. The cluster analyses applied to the grain size data allowed the distinction of five groups, named from C1 to C5, corresponding to progressively finer-grained and less sorted sediments (Fig. 6A).

**4.1.5. Crudely-layered sediments (middle slope)**

These light-grey sediments appear on the radiographs as vaguely stratified with little bioturbation. They contain mainly siliceous bioclasts (diatoms mud and ooze) and subordinately calcareous bioclasts (foraminifera and nanofossils) with rare, sparse IRD only at the base of the interval. The sediment density is low (1.5–1.6 g cm<sup>-3</sup>) with high water content (55% of wet weight) and weak shear strength (2–8 kPa, Fig. 4C). The sediment texture is fine-grained and consistent throughout

the core, with mean contents of 5% sand, 64% silt, 31% clay, and unimodal grain size spectra within the medium-grained silt fraction (Fig. 6B). This lithofacies was observed on the middle-slope cores only.

**4.1.6. Heavily-bioturbated sediments (middle slope)**

This facies is characterized by light-brown, very-low density, pervasively bioturbated, and bioclasts-rich sediments (mainly calcareous) lacking IRD content. The water content is the highest measured in the recovered cores (up to 60% of wet weight) with very weak shear strength (2–4 kPa, Fig. 4C). The sediment texture is fine-grained and generally very consistent through the lithofacies with mean contents of 4% sand, 67% silt, and 29% clay, and multimodal grain-size spectra suggesting low sorting (Fig. 6B). The heavily bioturbated sediments form the uppermost part of the middle-slope sequence (Fig. 4C).

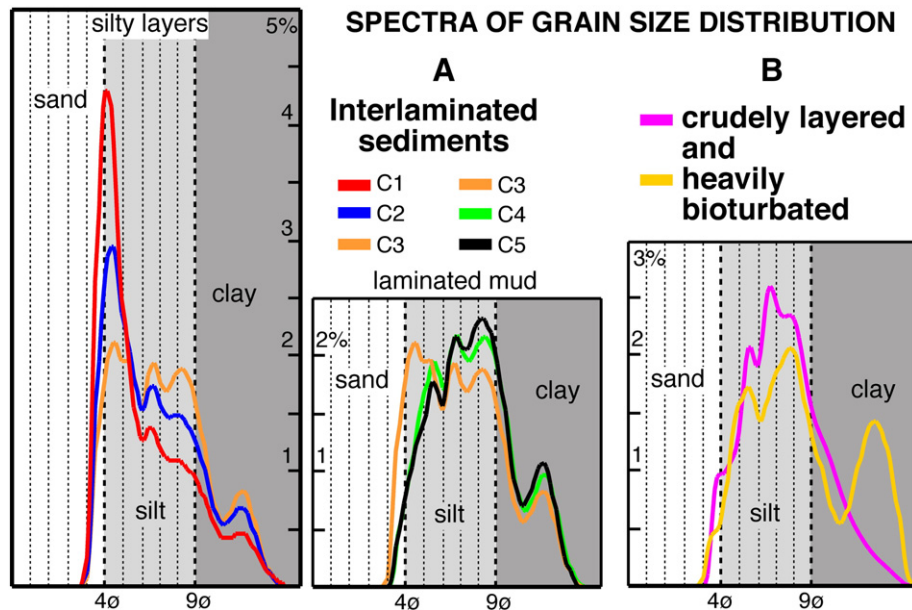


**Fig. 6.** Clusters of grain-size distribution spectra for (A) interlaminated sediments including sandy layers and laminated mud, and (B) crudely layered and heavily bioturbated sediments.

#### 4.1.7. Normally graded sands (upper slope)

A 20 cm thick normally graded sandy interval was recovered in the uppermost part of the trigger core SV-03tc (Fig. 4b). The sediments contain well rounded minerals and a large variety of bioclasts (foraminifera, nanofossils, diatoms, dyncocysts, ostracods). Thinner, massive sandy layers (1–3 cm thick) were observed at the top of the other upper slope cores (Fig. 4A, B).

#### 4.1.8. Clay mineral assemblage

The clay mineral assemblage on the Storfjorden TMF sediments is dominated by illite (always >50%), with variable percentages of chlorite (10–30%), kaolinite (10–20%), and generally small percentages or traces of smectite (0–18%, Fig. 4A, C). Following Junttila et al. (2010), we associated the illite, chlorite, and kaolinite contents with continental input deriving from subglacial erosion of the Fennoscandian Ice Sheet (cf. also Kuhelmann et al., 1993; Vogt and Knies, 2009), and the smectite is used as proxy for the NAC strength as originating from the hydrothermal alteration of the basalt of the Greenland-Faroe Ridge and Iceland-Vøring Plateau (cf. Love et al., 1989; Fagel et al., 2001), and transported to the area by the NAC. On the upper slope, the interlaminated sediments contain only traces of smectite that is virtually absent in the underlying stiff-massive diamicton (Fig. 4A). The smectite content increases up the sequence, having maximum values on the IRD-rich sediments outcropping on the upper slope (Fig. 4A). On the middle slope, the sediments contain a general higher amount of smectite with values peaking in the uppermost heavily-bioturbated sediments (Fig. 4C).

The  $C_{org}$  and the organic matter contents are maximum in the stiff diamicton of core SV-02 and in the slumped sediments of core SV-04, and minimum in the crudely-layered and heavily-bioturbated sediments at the top of the middle-slope sedimentary sequence (Fig. 4C).

#### 4.2. Micropaleontological content

On the upper slope, the sediments are almost barren except for the uppermost normally graded sands containing a rich biogenic association including diatoms, foraminifera, nanofossils, ostracods, and sponge spicules, indicating climatic conditions similar to present day in this high-latitude environment. Rare and often broken/reworked foraminifera were observed in the bioturbated-IRD-rich sediments, while the massive-IRD-rich sediments are barren except for a horizon located just above the stiff diamicton and characterized by a peak of Ca content (Fig. 4A, C).

On the middle-slope sediments, the biogenic association is generally richer especially within the uppermost heavily-bioturbated and crudely-layered sediments where bioclasts preservation is generally good. Diatoms are particularly abundant within the crudely-layered lithofacies. Their overall distribution is characterized by two distinct maxima centered 1) in the uppermost part of the heavily-bioturbated sediment, with an association dominated by *Chaetoceros RS* (resting spores) indicating high biological productivity, and 2) approximately in the middle part of the crudely-layered intervals, with an association dominated by *Coscinodiscus* spp. (warm conditions) and a group of species related with the North Atlantic Current, such as *Hemidiscus cuneiformis*, *Roperia tessellata*, *Azpeitia neocrenulata*, and *Thalassiosira oestrupii* (Fig. 4C). The latter peak marks the appearance and upward increase of calcareous bioclasts reaching their maximum abundance at the top of cores.

The calcareous nannoplankton assemblages at the base of the crudely-layered sediments is initially entirely formed by *Emiliania huxleyi*, soon after replaced by *Calcidiscus leptoporus* and *Gephyrocapsa oceanica* below the deeper diatoms peak in cores EG-03 and SV-04, and *Coccolithus pelagicus* above said peak where the assemblage indicate warm conditions.

The planktonic foraminifera assemblage is dominated by *Neogloboquadrina pachyderma* (s) although *Turborotalita quinqueloba* and *Neogloboquadrina pachyderma* (d) are abundant in the upper part of the cores. *Globigerina bulloides*, and *Globigerinita glutinata* represent

less than 8% of the total assemblage in most of the sediments. The benthic foraminifera group includes *Cassidulina reniforme* and *Cassidulina teretis* recovered in the coarse-massive-IRD facies above the interlaminated facies of core SV-04, whereas *Cibicidoides wuellerstorfi* and *Oridorsalis tener* were observed in the upper part of the bioturbated-IRD-rich facies, just below the crudely-layered lithofacies (Fig. 4C). In general, the concentration and distribution of the planktonic foraminifera have similar trends to that of coccoliths, with higher concentrations and diversifications in the middle slope heavily-bioturbated lithofacies.

#### 4.3. Core correlation and stratigraphy

Core correlation was based on the age model reconstructed by Sagnotti et al. (2011) using rock magnetic parameters with additional radiocarbon dating. The stratigraphic sequence is very consistent within each set of cores collected from the upper-slope and the middle-slope area. However, significant differences occur between the upper and middle slope sequences. The presence of red, oxidized layers was also considered as these layers consistently occur at the same stratigraphic level within the sequence (Fig. 7). Three oxidized layers were identified: OX-0, located at the sea surface and corresponding to the present oxy/redox interface; OX-1, located above the interlaminated lithofacies and recognized on the middle-slope cores only; and OX-2, located below the interlaminated facies and recognized on both the upper-slope cores and middle-slope core SV-04, that contains a continuous stratigraphic sequence back to 25 ka. The oxidized layers contain abundant Fe-oxides (mainly hematite), generating a sharp peak on the MS profile and on the green-red spectrum of sediment color (*index a*, Fig. 4A, C).

According to our chronostratigraphic reconstruction, the studied sediment cores record the post-LGM sedimentary sequence reaching, in some cases, the acoustic Unit C corresponding to the middle Weichselian interglacial MIS-3 (Pedrosa et al., 2011; Lucchi et al., 2012). A main stratigraphic discontinuity was identified in core EG-01, recovered from a minor gully of the upper slope (Fig. 4B), in which an erosive boundary separates interglacial MIS-3 sediments (32,792 cal. a BP) from interglacial MIS-1 sediments (ca 14 cal. ka BP). Other possible stratigraphic discontinuities were recorded at the top of the upper-slope core SV-03 between the interlaminated facies and the overlying bioturbated-IRD-rich sediments (inconsistency of depositional rates between the upper part of core SV-03 and the corresponding trigger core SV-03tc) and at the base of cores SV-03, SV-05, and SV-04 (sharp changes of physical and/or compositional characteristics).

An outstanding feature of the correlation scheme is that the upper slope sequence includes an extremely expanded interval corresponding to a short-lived sedimentary event represented by the interlaminated lithofacies.

The correlation scheme finds a good agreement with the stacked MS record produced for the West Svalbard margin by Jessen et al. (2010) and with the acoustic units identified by Pedrosa et al. (2011). The acoustically transparent Unit B is therefore formed by the stiff-massive diamicton lacking internal sedimentary structures. The laminated pattern of the acoustic facies A2 is due to the presence of sandy layers and layered IRD of the interlaminated and IRD-rich facies determining a strong reflectivity contrast within the bulk sediments. The youngest acoustic transparent facies A1 is associated with the homogeneous characteristics of the heavily-bioturbated and crudely-layered sediments of Holocene age (Fig. 7).

## 5. Discussion

### 5.1. Sedimentary processes on the Storfjorden and Kveithola TMFs

The presence of two distinct sedimentary sequences between the upper and middle-slope areas separated by only 35 km of distance, and the differences observed between the northern and southern parts of

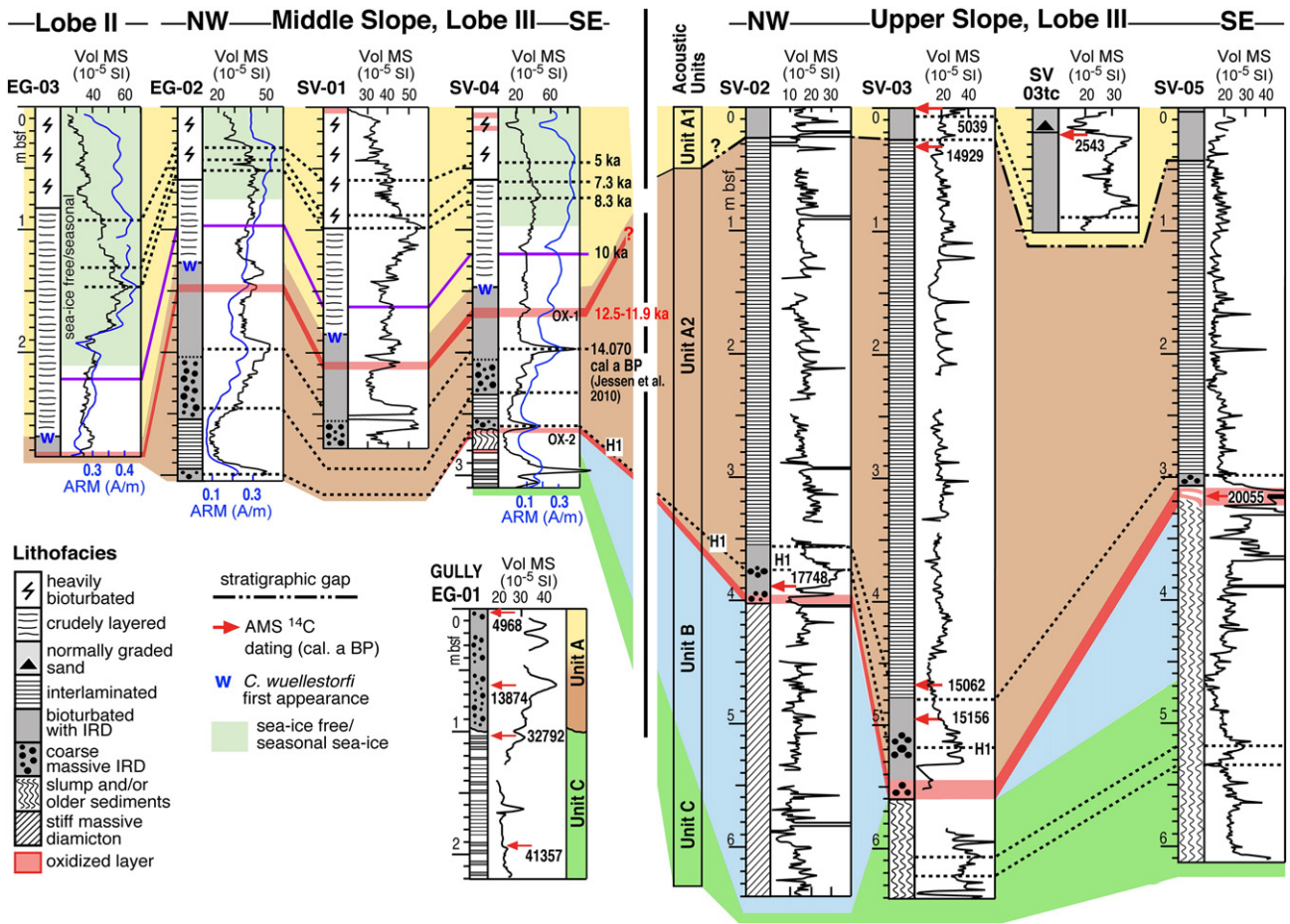


**Fig. 7.** Core correlation between the SVAIS and EGLACOM cores based of the age model generated by Sagnotti et al. (2011), lithofacies stratigraphy and the presence of the oxidized marker beds OX-1 and OX-2 (see text for discussion).

the middle-slope sequences, point to a strong across- and along-slope variability of the Storfjorden–Kveithola depositional system. The sedimentation on the upper slope appears strongly dominated by the input of continental derived sediments ( $C_{org}/N_{tot}$  ratio always  $\gg 10$ ). On the middle-slope area, most of the sedimentary record contains marine-derived organic matter and abundant bioclasts. Fig. 8 summarizes the physical and compositional characteristics of the lithofacies. A reconstruction of the recent depositional history of the Storfjorden–Kveithola TMFs depositional system is presented based on the recognized sedimentary processes whose onset appears closely tied to specific climatic conditions.

**5.1.1. LGM and early deglaciation**

The over-consolidated, stiff-massive diamicton recovered at the base of core SV-02, characterized by uniform physical and compositional characteristics without internal sedimentary structures, corresponds to a glacial diamicton (*sensu* Dowdeswell et al., 2000). In agreement with Laberg and Vorren (1996), Vorren and Laberg (1997), and Pedrosa et al. (2011), the presence of this type of deposit on the upper slope implies that the ice sheet was grounded at the shelf edge during the LGM. Contrarily to the glacial debris flows described by Laberg and Vorren (1995, 2000) and Laberg et al. (2012) on the middle-slope area of the Storfjorden and Bear Island TMFs that are characterized by medium-low shear strength, the high density and undrained shear strength measured on the stiff-massive diamicton of core SV-02 suggest little sediment remolding during the down-slope transport that possibly occurred as a rigid plug at least in the upper part of the slope where the deposit was retrieved.

The glacial diamicton represents episodes of fast deposition occurred during a very short period. The LGM stadial in the western Barents Sea is thought to have lasted a few thousand years, with chronology varying according to the data sets used: 24–23.5 cal. ka (Jessen et al., 2010); 23–19 cal. ka (Mangerud et al., 1998); 20–15 cal. ka (Svendsen et al., 2004); 19–15 cal. ka (Landvik et al., 1998). The thickness of the glacial diamicton, represented by acoustic Unit B, varies along the Storfjorden TMF from about 20 m off the southeastern Lobe III to over 45 m off the northwestern Lobe I. Assuming an average duration of 3 ka, the 45 m thick LGM diamicton was emplaced with an average sedimentation of  $1.5 \text{ cm a}^{-1}$ .

Other types of MTDs recovered in the area include water-rich, low-density debris flow/slumps (cores SV-04 and SV-05) that appear coeval with oxidized layer OX-2, suggesting slope instability occurred at the beginning of deglaciation, after the LGM.

The oxidized layer OX-2 is located at the base of the coarse-massive-IRD facies, just above the LGM glacial diamicton representing a widespread event recognized on the upper-slope and middle-slope sequences. Similar layers described from other areas of the Arctic Ocean are thought to derive from near-seabed oxidation of detrital Fe under interglacial well ventilated conditions (März et al., 2011). We therefore considered the oxidized layer OX-2 to mark the inception of deglaciation with release of fresh oxygenated waters ventilating bottom oceans in the Storfjorden area. According to dating, the onset of deglaciation on the Storfjorden TMF occurred around 20 cal. ka BP (core SV-05) and no later than 18 cal. ka BP (core SV-02), confirming the ages of 20–19 cal. ka BP suggested by Rasmussen et al. (2007) and Jessen et al. (2010).

Similarly to the stiff glacial diamicton, the coarse-massive-IRD facies overlying the LGM deposits contains organic-rich black shale

Sediment Lithofacies	STIFF-MASSIVE DIAMICTON	COARSE-MASSIVE IRD	INTERLAMINATED laminated mud and sandy layers		BIOTURBATED IRD-RICH	CRUDELY LAYERED	HEAVILY BIOTURBATED
X-radiograph							
Photograph							
sediment colour	very-dark grey	olive grey	MUD   SAND olive gray		grayish brown	light gray	light brown
bulk sediment density (g cc-1)	high 2.2	moderate 1.8	mid-low 1.7-1.8	high 2	low 1.6	very low 1.5-1.6	very low 1.4-1.5
water content (wet weight %)	<20	30	33	29	40	55-60	55-60
undrained shear strength	up to 44 kPa	20 kPa	4-12 kPa		6 kPa	2-8 kPa	2-4 kPa
mean grain size	matrix 6.5 $\phi$ M-silt & cm-thick pebbles	U.sl. 6.9 $\phi$ M-silt M.sl. 7.8 $\phi$ F-silt	7.5 $\phi$ F-silt	6.5 $\phi$ M-silt	6.8 $\phi$ M-silt	7.8 $\phi$ F-silt	7.7 $\phi$ F-silt
magnetic susceptibility	13 (10 <sup>-5</sup> SI)	15-30	15-20	up to 40	15-20	30	20-30
C <sub>org</sub> (%)	1.37	1.19	1.14		1.23	0.80	0.83
Org. Matter (%)	2.47	2.14	2.06		2.22	1.44	1.50
C <sub>org</sub> /N <sub>tot</sub> (OM provenance)	>12 continental	>12 continental	>12 continental	>12 cont. (U-slope) 8 marine (M-slope)	6-8 marine	6-8 marine	6-8 marine
CaCO <sub>3</sub> content (%)	4	3	2	3	2	7	13
smectite content (%)	absent	traces	4-10 upward increasing		11 off Lobe III 15 off Lobe II	12 off Lobe III 15 off Lobe II	13 15
microfossils	reworked bioclasts	almost barren	barren		rare bioclasts	mainly siliceous	calcareous and siliceous
setting	upper slope	upper + middle slope	upper + middle slope		upper + middle slope	middle slope	middle slope
Depositional Mechanism	SLOPE MTD OF GLACIGENIC DIAMICTON	GLACIMARINE WITH HIGH CALVING RATE	HIGH SUBGLACIAL DISCHARGE FROM MELTWATERS		GLACIMARINE WITH LOW CALVING RATE	CONTOUR CURRENTS WITH LITTLE BOTTOM   HIGH BOTTOM BIOLOGICAL ACTIVITY	
climatic stage	full glacial	early deglaciation & H1	MWP-1a		post MWP-1a & Younger Dryas	onset of interglacial	full interglacial

Fig. 8. Synthesis of the main lithofacies physical and compositional characteristics with inferred depositional mechanisms and relative timing of emplacement (see Discussion section for details). The values are reported as averages if not differently indicated. White/light-grey hues in the radiograph images correspond to high-density deposits.

fragments directly related to subglacial erosion. Differently, the presence of smectite in the clay mineral assemblage suggests increased influence of Atlantic waters on sedimentation. We associated the coarse-massive-IRD subfacies with a massive glaci-marine diamicton (*sensu* Dowdeswell et al., 2000) derived from increased calving rates in a warming environment (Clark et al., 2009). According to Zwally et al. (2002), the effects of climate warming on ice-sheets result in ice stream thinning and acceleration by subglacial melting with consequent increased calving rates. The presence of a foraminifera-rich interval located just above oxidized layer OX-2, characterized by marine-derived organic matter ( $C_{org}/N_{tot} < 10$ ), suggests renewed productivity under warmer, oxygen/nutrient-rich environmental conditions.

The onset of deglaciation on the Storfjorden glacial trough was shortly followed by a relatively cold period characterized by glacial stillstands or even ice streams re-advance to the outer areas of the glacial troughs (Pre-Bølling period) (Vorren and Plassen, 2002; Knies et al., 2007). Rùther et al. (2011) and Winsborrow et al. (2010) indicated a first ice stream re-advance on the neighboring Bjørnøyrenna glacial trough during 16.6–17.1 cal. ka BP. According to Jessen et al. (2010), evidences of such cold period on the West Spitsbergen are indicated by low sedimentation rates with low to moderate IRD concentrations. We associated the IRD-rich layer observed above the early deglaciation massive glaci-marine diamicton with Heinrich layer H1 (16.8 cal. ka BP) (Heinrich, 1988; Hemming, 2004), correlated among most of the cores and outlined by a peak of MS (Fig. 7).

#### 5.1.2. Onset of the main deglaciation phase: extensive meltwater release

The textural and compositional characteristics of the interlaminated facies recovered on the Storfjorden–Kveithola TMFs suggest deposition

occurred from prevailing subglacial meltwater plumes (*plumites*, *sensu* Hesse et al., 1997) with contour currents reworking of fines. The clay mineral analyses indicate a common continental origin for the laminated mud and the sandy layers with assemblages dominated by illite (across-slope transport) and only traces of smectite (along-slope advection). The percentage of smectite increases up-sequence and down-slope without a clear direct correlation with the distribution of the sandy layers or the laminated mud. A predominant across-slope continental input against lateral sediment advection is also supported by the high  $C_{org}/N_{tot}$  ratio and the presence of shelf derived glauconite in the sandy layers. The presence of layered IRD within the laminated mud is incompatible with across-slope deposition under turbidity currents due to the rapid emplacement mechanism of turbidites even thought to derive from low-density, distal turbidity flows (c.f. Wang and Hesse, 1996; Lucchi et al., 2002), and the regular, rhythmic recurrence of the sandy layers in the interlaminated sequence is inconsistent with turbidity currents associated with submarine slope instability. Contrarily, the co-existence of dispersed or layered IRD with sandy layers and/or the laminated mud, and the up-sequence and down-slope textural characteristics of the interlaminated facies are compatible with sedimentation from a retreating ice-front, similarly to the mechanism described for lacustrine glacial varves' formation (e.g., Breckenridge et al., 2012) or inner continental shelf terrigenous laminites/rhythmites/cyclopels (e.g., Mackiewicz et al., 1984; Stevens, 1990; Cowan et al., 1997, 1999; Cofaigh and Dowdeswell, 2001; Curran et al., 2004; Zajczkowski, 2008). Subglacial meltwater effluxes occur at the glacial grounding line, generating two main coupled density currents: a high-density underflow formed by the coarser-grained/heavier fraction that moves on the seafloor, having hydraulic characteristics of a hyperpycnal flow (Mulder

et al., 2003; Tripsanas and Piper, 2008), and a low-density buoyant overflow/inflow (hypopycnal flow) that spreads laterally, fan-shaped, on, or just below, the sea surface.

In core SV-02 from the upper slope, at 7 km from the shelf break, the sandy layers are initially 1–2 cm thick, very closely spaced, with massive or slightly graded sands over a sharp base. The grain size spectra indicate moderate to good sorting with unimodal spectra on the very-fine sand (cluster C1) suggesting a flow regime typical of relatively proximal areas (Mackiewicz et al., 1984; Cowan and Powell, 1990). The sandy layers' thickness, recurrence, and grain-size progressively decrease up the sequence, with textural characteristics indicating a progressive loss of flow competence, and sorting efficiency typical of more distal flow regimes (clusters C2, C3). Similarly, the laminated mud fines up-sequence having textural characteristics consistent with muddy contourites in the uppermost part of the sequence (poorly sorted, multimodal grain size spectra, Fig. 6). Higher percentages of smectite in the clay mineral assemblage confirm increased contribution of contour currents lateral advection of sediments. The interlaminated sediments recovered on the mid slope, at about 42 km from the shelf break, are only 15 cm thick (core SV-04), with textural and compositional characteristics similar to the upper part of the upper-slope sequence (clusters C4, C5), that is compatible with the modern distal plumites described by Mackiewicz et al. (1984) in the Muir inlet of Glacial Bay, Alaska, at 50 km away from the outflow.

The meter-thick sequence recovered on the upper slope thus records the progressive retreat inland of the ice sheet with seasonal delivery of coarser sediments (sandy layers) from relatively proximal to distal depositional conditions. The centimeter-thick sequence on the middle slope only records distal depositional conditions. The fine laminations observed in the sequence, are related to sediment reworking by persistent contour currents whose effect on sedimentation is initially completely overcome by the greater continental input by the turbid meltwaters.

Reduced IRD occurrence within the interlaminated sequence may be associated with the presence of extensive, multi-year sea ice preventing iceberg drift. On the middle slope, the interlaminated sequence is sharply overlaid by coarse-massive-IRD and bioturbated-IRD-rich sediments (Fig. 7). We associated the coarse-massive-IRD facies with the disintegration of the multi-year sea ice and further retreat of the Storfjorden ice stream. The predominance of *Cassidulina reniforme* and *Cassidulina teretis* in the benthic foraminifera assemblage of the coarse-massive-IRD interval confirm glacial conditions with relatively warm Atlantic water input (Hald and Korsun, 1997; Jennings et al., 2004). In the bioturbated-IRD-rich facies, the progressive fining-up of the bulk sediments and reduced occurrence of IRD was associated with distal glacial conditions (retreated calving line) with reduced continental sediment input by erratic icebergs. The oxidized layer OX-1 is recorded in this palaeoenvironmental scenario. According to our age model, the age of this sediment interval spans between 12.5 and 11.9 cal. ka BP, which conforms with the Younger Dryas cold pulse (12.9–11.7 cal. ka BP) (Broecker et al., 2010). The resolution of our analyses cannot solve the origin of the oxygenated waters responsible for this interval, which can, therefore, be either related to the inception of the Younger Dryas event (Keigwin and Jones, 1995; deVernal et al., 1996; Teller et al., 2002; and Broecker, 2006) or to its termination with release of meltwater similarly to oxidized layer OX-2. In either case, the little fine-grained IRD distribution in the correspondent sediments indicates the possible re-advance of the glacial terminus in the area, if any, did not affect the middle-slope sedimentation.

### 5.1.3. Holocene contour current sedimentation

Following the Younger Dryas cold event, the sedimentation on the middle-slope area, gradually changed to diatomaceous mud and ooze (crudely-layered lithofacies), indicating environmental conditions favorable to the primary productivity (Marchal et al., 2002; Martrat et al., 2003). This change is marked by the sudden appearance of the benthic foraminifera *Cibicidoides wuellerstorfi*, indicating a strong influx

of the North Atlantic waters (Rasmussen et al., 2007; Jessen et al., 2010). Crude bedding with sinusoidal laminations and unimodal grain size spectra suggests deposition under shear motions by low-energy currents. The bioturbation, mostly visible through radiographs, progressively increases up the sequence to become pervasive in the uppermost foraminifera bearing heavily-bioturbated facies. This latter facies contains sparse silty mottles and large burrows that completely obliterate the primary depositional structures with multimodal grain size spectra (Fig. 6). The consistent sediment texture throughout the sequence, the sediment composition with mixed hemipelagic-glaciomarine components, barren of shallow water bioclasts, and the high smectite content suggest deposition under hemipelagic conditions, with lateral sediment advection by Atlantic waters. Intense bioturbation and low  $C_{org}$  suggest strong benthonic bioactivity associated with well-oxygenated and nutrient-rich conditions compatible with contour current related environments (Stow and Holbrook, 1984; Chough and Hesse, 1985; Wetzel et al., 2008). This hypothesis is also supported by the highest benthic foraminifera diversity and concentration. We believe the described sequence corresponds to the intensively bioturbated muddy contourites described by Stow and Holbrook (1984) in North Atlantic sediments and Laberg and Vorren (2004) in the Lofoten contourite drift. Similarly to the latter, the possible origin of these contouritic sediments is due to along-slope sediment transport and deposition from intermediate water masses like the deep branch of the WSC (Blindheim, 1990; Beszczynska-Möller et al., 2012).

The lack of clear geophysical evidences of contouritic deposits on the present record of the Storfjorden apron is related to the reduced thickness of these deposits (1–2 m) that cannot be resolved with detail in the sub-bottom profiler data. The lack of contouritic deposits in the ancient record is related to episodic removal of interglacial sediments during the glacial stages, with massive glacial sediment input that obliterate previous slope morphologies. Slope-climbing sediment drifts were observed on the northern edge of the Storfjorden TMF in an area protected from episodic glacial diamicton input (Bellsund and Isfjorden drifts) (Rebesco et al., 2013). The origin of such deposits was related to combined along-slope Norwegian Sea deep waters episodically ventilated by relatively dense and turbid shelf waters from the Barents Sea, similar to the brine-enriched shelf waters presently forming on the Storfjorden inner area (Skogseth et al., 2005).

### 5.1.4. Recent emplacement of widespread gravity-mass deposits

The presence of isolated sandy turbidites in the uppermost part of the upper-slope sequence indicates episodes of slope instability in which the mechanisms of sediment re-deposition did not affected the middle-slope area. According to AMS  $^{14}C$  dating at the base of the sandy interval in core SV-03tc, the event occurred later than  $2543 \pm 73$  cal. ka BP. Sandy beds with a clear erosive base and containing broken shell debris were described from many cores along the neighboring Kveithola shelf, thought to have a regional distribution (Rüther et al., 2012). Erosional surfaces associated with stratigraphic hiatuses were observed also on the north-western part of the outer Storfjorden shelf (core SV-06) (Sagnotti et al., 2011) having similar timing to those described in the Kveithola shelf and thus sustaining the widespread, regional character of such features. Rüther et al. (2012) speculate that the recorded hiatuses and the bases of the sand units are time correlated with recognized large tsunami-triggering landslides documented in the Norwegian-Barents Sea.

### 5.2. Stratigraphic and morphological structures associated to deglaciation

The lithostratigraphic characteristics of the upper-slope cores suggest that deglaciation on the Storfjorden–Kveithola glacial troughs was driven by grounded ice lift-off with consequent rapid ice stream retreat from the continental shelf edge. The effects of deglaciation left two important imprints on the continental slope morphology and depositional architecture: the incision of a dense network of gullies developing from the upper slope and the deposition of a thick interlaminated

sequence. Both features were related to extensive, powerful, release of subglacial turbid meltwaters.

### 5.2.1. Gullies formation

High-energy subglacial jet-flows consisting of mixed fresh meltwater and glacial sediments released under high hydrostatic head near the base of the water column (Syvitski, 1989; Powell, 1990) were responsible for localized substrate erosion at the ice streams' terminus. Studies conducted on the modern tidewater glaciers' fjords depositional systems indicate that the erosive efficiency of these jet-flows is maximum near the efflux area (grounding line) and rapidly decreases with distance from the ice terminus as the dynamic and physical characteristics of the flows change from high-density, laminar flows to progressively lower density, turbulent flows due to ambient fluid entrainment. According to Powell (1990), the coarsest bed-load settles close to the efflux area, generating transverse sediment ridges during the ice sheet retreat (e.g., grounding-zone wedges of Kveithola Trough) (Rebesco et al., 2011), while gravel and sands are transported further away through hyper-concentrated flows that move in contact with the seafloor generating bottom scour features. The runoff distance of jet-flows is a function of their initial momentum, the sediment load concentration, and density differences with the ambient fluid. Maximum erosive efficiency of the jet-flows on the upper slope must have occurred at the very beginning of the deglaciation when the ice streams were still grounded at the shelf break and the low sea level produced the highest hydrostatic head. Differently from modern fjord systems characterized by almost flat bathymetry, the runoff distance on the Storfjorden and Kveithola TMFs was possibly enhanced by the over-steepened uppermost slope formed by amalgamated till deltas with high friction angle (Pedrosa et al., 2011). The main stratigraphic discontinuity observed in core EG-01 is associated with sediment erosion and/or non-deposition within a upper-slope gully (Fig. 4b). The presence of a scoured boundary between acoustic Unit C (32.8 cal. ka BP) and Unit A (14 cal. ka BP) suggests that meltwater erosion during early deglaciation removed not only the glacial sedimentation, but also part of the older sequence, preventing deposition of the sediments associated with the main deglaciation phase (interlaminated facies). The sub-bottom profiler record indicates that numerous gullies were excavated through the stiff glacial diamicton, suggesting high efficiency of this erosive process on the upper slope (Pedrosa et al., 2011).

### 5.2.2. Stratigraphic significance and environmental impact of massive, rapid glacimarine sedimentation

The high sedimentation rate calculated for the interlaminated sequence on the upper slope suggests that deposition occurred from a high discharge meltwater system in which the coarser fraction rains out from the buoyant vertical plume generating an hyperpycnal flow responsible for the deposition of a veil of coarser sediments (sandy layers) while fines rise to the level of neutral buoyancy forming a hypopycnal flow from which particles flocculate to settle vertically (Powell, 1990; Mugford and Dowdeswell, 2011). Over 4.5 m of interlaminated sediments were deposited in less than 150 years, at 7 km from the shelf break (core SV-03), suggesting a massive sediment input accompanied by a huge flux of fresh meltwater. Equivalent postglacial interlaminated deposits have been reported along the West Svalbard continental slope and outer shelf dated 14.7–14.4 cal. ka BP (Elverhøi et al., 1995; Rasmussen et al., 2007; Jessen et al., 2010) in the Kveithola through (Rüther et al., 2012) and in the southern Barents Sea (Vorren et al., 1984), representing a nearly synchronous regional event.

We propose that the interlaminated sediments recovered on the Storfjorden TMF slope represent the high-latitude marine record of meltwater pulse 1a (MWP-1a), representing one of the most dramatic ice melting events of the last deglaciation responsible for an abrupt sea level rise of about 20 m within a few hundred years (Fairbanks, 1989; Clark et al., 1996; Hanebuth et al., 2000; Clark et al., 2002a; Alley et al., 2005; Peltier, 2005; Rinterknecht et al., 2006).

Such a huge, nearly instantaneous meltwater event recorded in our sediment cores, is constrained by an excellent palaeomagnetic and stratigraphic correlation with the sedimentary sequences described west of Svalbard and neighboring glacial trough depositional systems (Jessen et al., 2010) where radiocarbon ages fits with the timing of MWP-1a (Deschamps et al., 2012). The slightly older ages determined in our cores with respect to the established timing for MWP-1a can be related to underestimation of the local regional reservoir correction applied to radiocarbon dating calibration. In fact, regional reservoir corrections are determined for surface waters whereas our samples included a large part of benthic fauna. According to Sarnthein (2011), deep waters between the LGM and Heinrich Stage 1 (HS1) were, on average, 1000–2000 y older than they are today, leading to a higher local reservoir age.

There is still an open debate on the trigger mechanism(s) and the source area for MWP-1a (e.g., Clark et al., 2002b, 2009; Weaver et al., 2003; Rinterknecht et al., 2006; Stanford et al., 2006; Weber et al., 2011; Kopp, 2012); however, there is consensus on a significant southern hemisphere contribution for such outstanding global sea level rise. According to Clark et al. (2009), the enhanced northern insolation was the primary mechanism for triggering the onset of the northern hemisphere deglaciation (21–19 cal. ka BP). The loss of mass of the Laurentide and Fennoscandian ice-sheets and the mountain glaciers melting in the northern hemisphere produced large volume of meltwater with deposition, on the northern continental margins, of a thick laminated sequence (ca. 21–18 cal. ka BP) (Lekens et al., 2005; Tripsanas and Piper, 2008). This initial phase of deglaciation was responsible for a first abrupt sea level rise (19 ka-MWP, 10–15 m) (Clark et al., 2004; Rinterknecht et al., 2006) triggering the lift-off and subsequent melting of the marine-based grounded ice streams in the Weddell and Amundsen Seas, with deposition of a thick terrigenous laminated sequence underneath the correspondent Antarctic ice-shelves (Weber et al., 2011). According to Weaver et al. (2003), meltwater release from the Western Antarctic Ice Sheet would have strengthened the Atlantic meridional overturning circulation accelerating the climate warming of the North Atlantic region (onset of the Bølling–Allerød warm interval). At the same time, Antarctic freshwater release forcing sea level rise was responsible for lift-off of some shallower marine grounded ice streams in the northern margins including the Storfjorden and Kveithola ice streams, with their consequent rapid melting and retreat to an inner grounding line, contributing significantly to the sea level rise during MWP-1a. Palaeoceanographic studies indicate, and confirm, that a strong correlation exists between the dynamics of the Svalbard–Barents Sea Ice Sheet and the flow of NAC over the Svalbard margin (Martrat et al., 2003; Rasmussen et al., 2007; Jessen et al., 2010). Subglacial inflow of warm North Atlantic waters forced rapid melting and retreat of the Storfjorden ice stream after its lift-off, similarly to meltwater forcing effects of sub-ice-shelf warm currents in Antarctica (Shepherd et al., 2003).

The thickness of the Storfjorden interlaminated facies varies not only with distance from the shelf break but also along the slope. Sub-bottom profiler records revealed thicker laminated acoustic facies in the recent and older sequence of the SE area of the Storfjorden (lobe III) and Kveithola TMFs with respect to the central and northeastern area of Storfjorden (Lobes II and I) (Pedrosa et al., 2011). According to Hesse et al. (1997), the seaward limit for plumites is on the order of a few tens of kilometers from the ice-sheet terminus, which would imply a prolonged residence of the southeast ice streams' terminus at or nearby the shelf break during the ice sheet retreat after LGM.

On the Storfjorden Trough a first ice sheet stabilization line was preliminarily identified from regional bathymetric data at about 75 km east of the shelf break (Fig. 9 and Bathymetric Step, BS in Fig. 3 of Pedrosa et al., 2011), whereas on the Kveithola Trough the two deeper GZWs are located at only 20 and 37 km east of the shelf break (Fig. 9). A combination of factors probably allowed the ice stream to persist longer in the area close to the shelf break in the southwestern Storfjorden and Kveithola Troughs: i) The bathymetric characteristics of the two troughs,

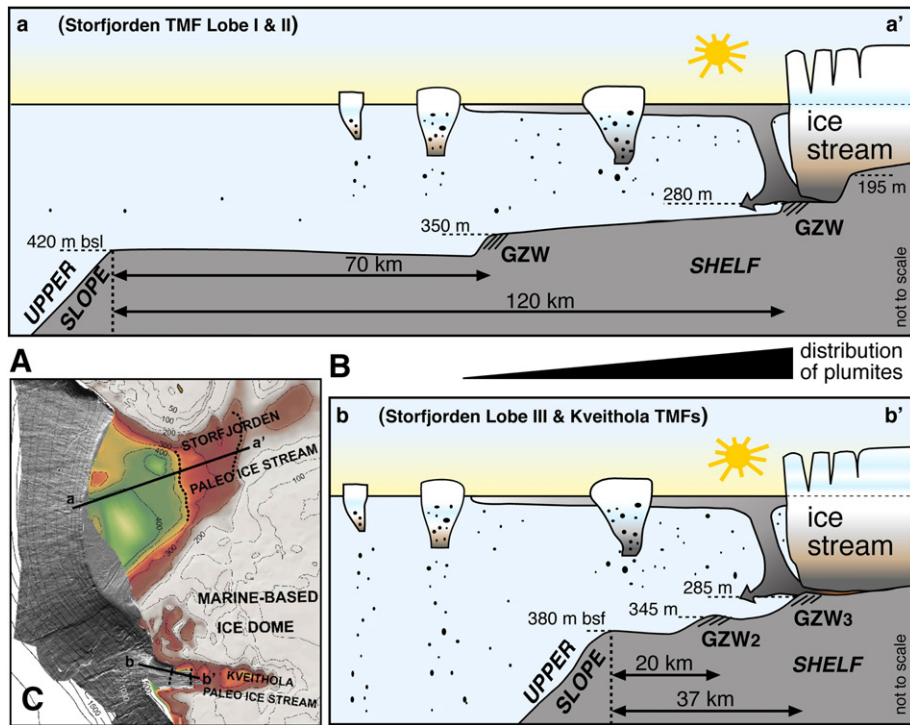


**Fig. 9.** Conceptual scheme of the ice stream retreat on the Storffjorden (A) and Kveithola (B) troughs. (C) Bathymetric map as in Fig. 2, indicating the location of the two cross sections of figures (A) and (B) and the location of the Grounding Zone Wedges (GZW) where the ice-streams stepped during the retreat.

being the Kveithola shallower and steeper than the Storffjorden through; ii) The proximal location of the ice catchment area of the southwestern Storffjorden originating from the local Spitsbergenbanken ice cap (Fig. 2 in Pedrosa et al., 2011); and iii) The flow path of warm surface Atlantic currents being possibly deflected offshore by the Spitsbergenbanken promontory (no traces of WSC-derived smectite in the Kveithola shelf sedimentary sequence, indicating minor influence of Atlantic waters inflow) (Rüther et al., 2012). A stronger influence of Atlantic waters to the northern Storffjorden area with respect to the southern part is supported by the consistently higher values of smectite throughout the former sedimentary sequence (Figs. 4A, C, 8), and the Holocene nannofossil distribution on the middle-slope sediment sequence confirm that ice-free/seasonal conditions occurred earlier in the northern area with respect to the southern part (Fig. 7).

The different bathymetric characteristics of Storffjorden and Kveithola Troughs likely determined a different amplitude of the initial ice stream lift-off, with a more inland, retreated location of the northwestern part of the Storffjorden grounding line with respect to that of Kveithola (Fig. 9). Turbid meltwater plumes released at glacial terminus located some 60–70 km inland could not reach the continental slope, depositing on the continental shelf (Fig. 9).

It is also possible that the Storffjorden Lobe III slope received additional suspended sediments from the ice melting of the adjacent Kveithola ice stream or the marine-based Spitsbergenbanken ice dome. According to Rüther et al. (2012) and Bjarnadóttir et al. (2013), the ca 100 m long Kveithola trough was deglaciated by the end of MWP-1a (14.2 cal. ka BP), and thus it is likely that the retreat of the Kveithola ice stream released a large amount of sediment during the main phase of meltwater pulse 1a. The turbid meltwater plumes could have drifted to the Storffjorden area by the surface West Spitsbergen Current, similarly to the modern Nordaustlandet tidewater ice cap outflow system in which summer suspended turbid plumes extend about 15 km perpendicular to the glacier outlet and approximately 60 km away along the ice front being deflected and transported by surface currents (Pfirman and Solheim, 1989). Fohrmann et al. (1998), indicate the SE area of

Storffjorden slope (lobe III) as depocentre for the sediment-enriched brines that periodically spill over the Kveithola shelf break and are drifted north-eastwards by the local current's pattern.

## 6. Conclusions

Sedimentation in Storffjorden and Kveithola TMF area changed with time and space being related to bathymetric, glaciological, and oceanographic factors whose interaction determines drastically different styles of sedimentary architecture within the same TMF.

Five main sedimentary facies were associated with onset of climatically driven depositional mechanisms including (1) massive transport of high-density, low shear strength glaciogenic debris flows (stiff-massive diamicton), which gives an indication of ice streams grounded at the shelf edge during maximum glacial advance; (2) massive delivery of IRD-rich sediments associated with initial climatic warming with enhanced calving rate; (3) massive sediment input associated with rapid ice stream melting and retreat (interlaminated sediments, plumites); (4) crudely-layered; and (5) heavily-bioturbated sediments deposited by contour currents during progressively ameliorated climatic/environmental conditions favorable to the biological productivity.

Two intervals of red, oxidized sediments were associated with release of cold oxygenated waters, marking, in the studied cores, the post LGM inception of deglaciation, and the Younger Dryas climatic interval.

According to chronostratigraphic and sedimentological characteristics, the thick plumite sequence recovered on the upper slope represents an extreme depositional event associated with an outstanding glacial meltwater phase. We propose such deposits to likely represent the high-latitude marine sedimentary record of MWP-1a.

Different bathymetric and oceanographic conditions controlled the local mode of glacial retreat during MWP-1a, resulting in different thickness of plumites along the Storffjorden upper slope. It is possible that the southern part of Storffjorden TMF received additional sediments from the deglaciation of the neighboring Kveithola ice stream.

## Acknowledgements

This study was supported by the Spanish IPY projects SVAIS (POL2006-07390/CGL) and IPY-NICE STREAMS (CTM2009-06370-E/ANT), the Spanish project DEGLABAR (CTM2010-17386), and the Italian projects OGS-EGLACOM, and PNRA-MELTSTORM. We thank ENI E&P Division (Milan, Italy) for the analysis with the X-ray CT scan, MARUM laboratory for the use of the XRF core-scan, and CMIMA (CSIC-Barcelona) for the analyses with multi-sensor core logger. Technical/scientific support was given by M. Quart and J. Frigola (University of Barcelona), and V. Lukes (MARUM-Bremen). We thank two anonymous reviewers and the editor T. Cronin, for critical reading of the manuscript and for suggestions that greatly improved the manuscript.

## References

- Alley, R.B., Blankenship, D.D., Rooney, S.T., Bentley, C.R., 1989. Sedimentation beneath ice shelves—the view from ice stream B. *Mar. Geol.* 85, 101–120.
- Alley, R.B., Clack, P.U., Huybrechts, P., Jounghin, I., 2005. Ice-sheet and sea-level changes. *Science* 310, 456–460.
- Andreassen, K., Laberg, J.S., Vorren, T.O., 2008. Seafloor geomorphology of the SW Barents Sea and its glaci-dynamic implications. *Geomorphology* 97, 157–177.
- Backman, J., Fornaciari, E., Rio, D., 2009. Biochronology and paleoceanography of late Pleistocene and Holocene calcareous nannofossils across the Arctic Basin. *Mar. Micropaleontol.* 72, 86–98.
- Beszczynska-Möller, A., Fahrbach, E., Schauer, U., Hansen, E., 2012. Variability in Atlantic water temperature and transport at the entrance to the Arctic Ocean, 1997–2010. *ICES J. Mar. Sci.* 69, 852–863.
- Biscay, P.E., 1965. Mineralogy and sedimentation of recent deep-sea clay in Atlantic Ocean and adjacent seas and oceans. *Geol. Soc. Am. Bull.* 76, 803–832.
- Bjarnadóttir, L.R., Rütther, D.C., Winsborrow, M.C.M., Andreassen, K., 2013. Grounding-line dynamics during the last deglaciation of Kveithola, W Barents Sea, as revealed by seabed geomorphology and shallow seismic stratigraphy. *Boreas* 42, 84–107.
- Blindheim, J., 1990. Arctic intermediate water in the Norwegian Sea. *Deep-Sea Res.* 37, 1475–1489.
- Breckenridge, A., Lowell, T.V., Stroup, J.S., Evans, G., 2012. A review and analysis of varve thickness records from glacial Lake Ojibway (Ontario and Quebec, Canada). *Quat. Int.* 26, 43–54.
- Broecker, W.S., 2006. Was the Younger Dryas triggered by a flood? *Science* 312, 1146–1148. <http://dx.doi.org/10.1126/science.1123253>.
- Broecker, W.S., Denton, G.H., Edward, R.L., Cheng, H., Alley, R.B., 2010. Putting the Younger Dryas cold event into context. *Quat. Sci. Rev.* 29, 1078–1081.
- Butt, F.A., Drange, H., Elverhøi, A., Otterå, O.H., Solheim, A., 2002. Modelling late Cenozoic isostatic elevation changes in the Barents Sea and their implications for oceanic and climatic regimes; preliminary results. *Quat. Sci. Rev.* 21, 1643–1660.
- Chough, S.K., Hesse, R., 1985. Contourites from Eirik Ridge, South of Greenland. *Sediment. Geol.* 41, 185–199.
- Clark, P.U., Alley, R.B., Keigwin, L.D., Licciardi, J.M., Johnsen, S.J., Wang, H., 1996. Origin of the first global meltwater pulse following the Last Glacial Maximum. *Paleoceanography* 11, 563–577.
- Clark, P.U., Mitrovica, J., Milne, G., Tamisiea, M., 2002a. Sea level fingerprinting as a direct test for the source of global melt water pulse 1 A. *Science* 295, 2438–2441.
- Clark, P.U., Pisias, N.G., Stocker, T.F., Weaver, A.J., 2002b. The role of the thermohaline circulation in abrupt climate change. *Nature* 415, 863–869.
- Clark, P.U., McCabe, A.M., Mix, A.C., Weaver, A.J., 2004. Rapid rise of sea level 19,000 years ago and its global implications. *Science* 304, 1141–1144.
- Clark, P.U., Arthur, S.D., Shakun, J.D., Carlson, A.E., Clark, J., Wohlfarth, B., Mitrovica, J.X., Hostetler, S.W., McCabe, A.M., 2009. The Last Glacial Maximum. *Science* 325, 710.
- Cofaigh, Ó.C., Dowdeswell, J.A., 2001. Laminated sediments in glacial marine environments: diagnostic criteria for their interpretation. *Quat. Sci. Rev.* 20, 1411–1436.
- Cofaigh, Ó.C., Taylor, J., Dowdeswell, J.A., Pudsey, C.J., 2003. Palaeo-ice streams, trough mouth fans and high-latitude continental slope sedimentation. *Boreas* 32, 37–55.
- Cowan, E.A., Powell, R.D., 1990. Suspended sediment transport and deposition of cyclically interlaminated sediment in a temperate glacial fjord, Alaska, USA. In: Dowdeswell, J.A., Scourse, J.D. (Eds.), *Glacial Marine Environments: Processes and Sediments*. Geological Society Special Publication, 53, pp. 75–89.
- Cowan, E.A., Cai, J., Powell, R.D., Clark, J.D., Pitcher, J.N., 1997. Temperate glacial marine varves: an example from Disenchantment Bay, Southern Alaska. *J. Sediment. Res.* 67, 536–549.
- Cowan, E.A., Seramur, K.C., Cai, J., Powell, R.D., 1999. Cyclic sedimentation produced by fluctuations in meltwater discharge, tides and marine productivity in an Alaskan fjord. *Sedimentology* 46, 1109–1126.
- Curran, K.J., Hill, P.S., Milligan, T.G., Cowan, E.A., Syvitski, J.P.M., Konings, S.M., 2004. Fine-grained sediment flocculation below the Hubbard Glacier meltwater plume, Disenchantment Bay, Alaska. *Mar. Geol.* 20, 83–94.
- Deschamps, P., Durand, N., Bard, E., Hamelin, B., Camoin, G., Thomas, A.L., Henderson, G.M., Okuno, J., Yokoyama, Y., 2012. Ice-sheet collapse and sea-level rise at the Bølling warming 14,600 years ago. *Nature* 483, 559–564.
- deVernal, A., Hillaire-Marcel, C., Bilodeau, G., 1996. Reduced meltwater outflow from the Laurentide ice margin during the Younger Dryas. *Nature* 381, 774–777. <http://dx.doi.org/10.1038/381774a0>.
- Dowdeswell, J.A., Whittington, R.J., Jennings, A.E., Andrews, J.T., Mackensen, A., Marienfeld, P., 2000. An origin for laminated glacial marine sediments through sea-ice build-up and suppressed iceberg rafting. *Sedimentology* 47, 557–576.
- Dowdeswell, J.A., Ottesen, D., Evans, J., Cofaigh, Ó.C., Anderson, J.B., 2008. Submarine glacial landforms and rates of ice-stream collapse. *Geology* 36, 819–822.
- Dowdeswell, J.A., Hogan, K.A., Evans, J., Noormets, R., Cofaigh, Ó.C., Ottesen, D., 2010. Past ice-sheet flow east of Svalbard inferred from streamlined subglacial landforms. *Geology* 38, 163–166.
- Ehrmann, W., Melles, K., Kuhn, G., Grobe, H., 1992. Significance of clay mineral assemblages in the Antarctic Ocean. *Mar. Geol.* 107, 249–273.
- Elverhøi, A., Andersen, E.S., Dokken, T., Hebbeln, D., Spielhagen, R., Svendsen, J.I., Sørflaten, M., Rørnes, A., Hald, M., Forsberg, C.F., 1995. The growth and decay of the Late Weichselian ice sheet in western Svalbard and adjacent areas based on provenance studies of marine sediments. *Quat. Res.* 44, 303–316.
- Fagel, N., Robert, C., Preda, M., Thorez, J., 2001. Smectite composition as tracer of deep circulation: the case of Northern North Atlantic. *Mar. Geol.* 172, 309–330.
- Fairbanks, R.G., 1989. A 17,000-year glacio-eustatic sea level record: influence of glacial melting rates on the Younger Dryas event and deep-ocean circulation. *Nature* 342, 637–642.
- Feyling-Hanssen, R.W., Jørgensen, J.A., Knudsen, K.L., Andersen, A.-L., 1971. Late Quaternary Foraminifera from Vendsyssel, Denmark and Sandnes, Norway. *Bull. Geol. Soc. Den.* 21, 67–317.
- Fohrmann, H., Backhaus, J.O., Blaume, F., Rumohr, J., 1998. Sediments in bottom-arrested gravity plumes: numerical case studies. *J. Phys. Oceanogr.* 28, 2250–2274.
- Friedman, G.M., Sanders, J.E., 1978. *Principles of Sedimentology*. John Wiley & Sons, New York (792 pp.).
- Geyer, F., Ferc, I., Eldevik, T., 2009. Dense overflow from an Arctic fjord: Mean seasonal cycle, variability and wind influence. *Cont. Shelf Res.* 29, 2110–2121.
- Gordon, D.C., 1970. A microscopic study of organic particles in the North Atlantic Ocean. *Deep-Sea Res.* 17, 175–185.
- Hald, M., Korsun, S., 1997. Distribution of modern benthic foraminifera from fjords of Svalbard, European Arctic. *J. Foramin. Res.* 27, 101–122.
- Hanebuth, T., Statteger, K., Grootes, P.M., 2000. Rapid flooding of the Sunda Shelf: a Late-Glacial sea-level record. *Science* 288, 1033–1035.
- Heinrich, H., 1988. Origin and consequences of cyclic ice rafting in the northeast Atlantic Ocean during the past 130,000 years. *Quat. Res.* 29, 142–152.
- Hemleben, C., Spindler, M., Anderson, O.R., 1989. *Modern Planktonic Foraminifera*. Springer Verlag, Berlin (363 pp.).
- Hemming, S.R., 2004. Heinrich events: massive late Pleistocene detritus layers of the North Atlantic and their global climate imprint. *Rev. Geophys.* 42, RG1005. <http://dx.doi.org/10.1029/2003RG000128>.
- Hesse, R., Khodabakhsh, S., Klauk, I., Ryan, W.B.F., 1997. Asymmetrical turbid surface-plume deposition near ice-outlets of the Pleistocene Laurentide ice sheet in the Labrador Sea. *Geo-Mar. Lett.* 17, 179–187.
- Hine, N., Weaver, P.P.E., 1998. *Quaternary*. In: Bown, P.R. (Ed.), *Calcareous Nannofossil Biostratigraphy*. Kluwer Academic Publishers, Dordrecht, pp. 266–283.
- Hjelstuen, B.O., Elverhøi, A., Faleide, J.I., 1996. Cenozoic erosion and sedimentary yield in the drainage area of the Storfjorden Fan. *Glob. Planet. Chang.* 12, 95–116.
- Jennings, A.E., Weiner, N.J., Helgadottir, G., Andrews, J.T., 2004. Modern foraminiferal faunas of the southwestern to northern Iceland shelf: oceanographic and environmental controls. *J. Foraminif. Res.* 34, 180–207.
- Jessen, S.P., Rasmussen, T.L., Nielsen, T., Solheim, A., 2010. A new Late Weichselian and Holocene marine chronology for the western Svalbard slope 30,000–0 cal years BP. *Quat. Sci. Rev.* 29, 1301–1312.
- Junttila, J., Aagaard-Sørensen, S., Husum, K., Hald, M., 2010. Late Glacial–Holocene clay minerals elucidating glacial history in the SW Barren Sea. *Mar. Geol.* 276, 71–85.
- Keigwin, L.D., Jones, G.A., 1995. The marine record of deglaciation from the continental margin off Nova Scotia. *Paleoceanography* 10, 973–985. <http://dx.doi.org/10.1029/95PA02643>.
- Knies, J., Vogt, C., Matthiessen, J., Nam, S.-I., Ottesen, D., Rise, L., Bargel, T., Eilertsen, R.S., 2007. Re-advance of the Fennoscandian Ice Sheet during Heinrich Event 1. *Mar. Geol.* 240, 1–18.
- Kopp, R.E., 2012. Palaeoclimate: Tahitian record suggests Antarctic collapse. *Nature* 483, 549–550.
- Kuhelmann, J., Lange, H., Peatsch, H., 1993. Implications of a connection between clay mineral variations and coarse grained debris and lithology in the central Norwegian–Greenland Sea. *Mar. Geol.* 114, 1–11.
- Laberg, J.S., Vorren, T.O., 1995. Late Weichselian submarine debris flow deposits on the Bear Island Trough Mouth Fan. *Mar. Geol.* 127, 45–72.
- Laberg, J.S., Vorren, T.O., 1996. The glacier-fed fan at the mouth of Storfjorden trough, western Barren Sea: a comparative study. *Geol. Rundsch.* 85, 338–349.
- Laberg, J.S., Vorren, T.O., 2000. Flow behaviour of the submarine glacial debris flows on the Bear Island Trough Mouth Fan, western Barents Sea. *Sedimentology* 47, 1105–1117.
- Laberg, J.S., Vorren, T.O., 2004. Weichselian and Holocene growth of the northern high-latitude Lofoten Contourite Drift on the continental slope of Norway. *Sediment. Geol.* 164, 1–17.
- Laberg, J.S., Stoker, M.S., Dahlgren, K.I.T., de Haas, H., Hafidason, H., Hjelstuen, B.O., Nielsen, T., Shannon, P.M., Vorren, T.O., van Weering, T., Ceramicola, S., 2005. Cenozoic along slope processes and sedimentation on the NW European Atlantic margin. *Mar. Pet. Geol.* 22, 1069–1088.
- Laberg, J.S., Andreassen, K., Knies, J., Vorren, T., Winsborrow, M., 2010. Late Pliocene–Pleistocene development of the Barents Sea Ice Sheet. *Geology* 38, 107–110. <http://dx.doi.org/10.1130/G30193.1>.
- Laberg, J.-S., Johansen, R., Bünz, S., 2012. A surging behaviour of glacial debris flows. In: Yamada, Y., Kawamura, K., Ikehara, K., Ogawa, Y., Urgeles, R., Mosher, D., Chaytor, J., Strasser, M. (Eds.), *Submarine Mass Movements and Their Consequences*.

- Advances in Natural and Technological Hazards Research, Springer Science book series, 31, pp. 159–166.
- Landvik, J.Y., Bondevik, S., Elverhøi, A., Fjeldskaar, W., Mangerud, J., Salvigse, O., Siegert, M.J., Svendsen, J.I., Vorren, T.O., 1998. The last glacial maximum of Svalbard and the Barents Sea area: ice sheet extent and configuration. *Quat. Sci. Rev.* 17, 43–75.
- Lekens, W.A.H., Sejrup, H.P., Hafliðason, H., Petersen, G.Ø., Hjelstuen, B., Knorr, G., 2005. Laminated sediments preceding Heinrich event 1 in the Northern North Sea and Southern Norwegian Sea: Origin, processes and regional linkage. *Mar. Geol.* 216, 27–50.
- Leroueil, S., Le Bihan, J.P., 1996. Liquid limits and fall cones. *Can. Geotech. J.* 33, 793–798.
- Loeblich, A.R., Tappan, H., 1987. Foraminiferal Genera and Their Classification (2 vols). Van Nostrand Rienhold Co., New York (970 pp. (vol. 1), 213 pp. (vol.2), 847 plates).
- Love, D.A., Frappe, S.K., Gibson, I.L., Jones, M.G., et al., 1989. The  $\delta^{18}\text{O}$   $\delta^{13}\text{C}$  isotopic composition of secondary carbonates from basaltic lavas cored in Hole 642E. Ocean Drilling Program Leg 1041. In: Eldholm, O., Thiede, J., Taylor, E. (Eds.), Proceedings of the Ocean Drilling Program. Scientific Results, 104. Ocean Drilling Program, College Station TX, pp. 449–455.
- Lucchi, R.G., Rebesco, M., Camerlenghi, A., Busetti, M., Tomadin, L., Villa, G., Persico, D., Morigi, C., Bonci, M.C., Giorgetti, G., 2002. Glacimarine sedimentary processes of a high-latitude, deep-sea sediment drift (Antarctic Peninsula Pacific margin). *Mar. Geol.* 189, 343–370.
- Lucchi, R.G., Pedrosa, M.T., Camerlenghi, A., Urgeles, R., De Mol, B., Rebesco, M., 2012. Recent submarine landslides on the continental slope of Storfjorden and Kveithola Trough-Mouth Fans (north west Barents Sea). In: Yamada, Y., Kawamura, K., Ikehara, K., Ogawa, Y., Urgeles, R., Mosher, D., Chaytor, J., Strasser, M. (Eds.), Submarine Mass Movements and Their Consequences. Advances in Natural and Technological Hazards Research, Springer Science book series, 31, pp. 735–745.
- Mackiewicz, N.E., Powell, R.D., Carlson, P.R., Molnia, B.F., 1984. Interlaminated ice-proximal glacial marine sediments in Muir inlet, Alaska. *Mar. Geol.* 57, 113–147.
- Mangerud, J., Dokken, T., Hebbeln, D., Heggen, B., Ingólfsson, Ó., Landvik, J.Y., Mejdahl, V., Svendsen, J.I., Vorren, T.O., 1998. Fluctuations of the Svalbard–Barents sea ice sheet during the last 150,000 years. *Quat. Sci. Rev.* 17, 11–42.
- Marchal, O., Cacho, I., Stocker, T.F., Grimalt, J.O., Calvo, E., Martrat, B., Shackleton, N., Vautravers, M., Cortijo, E., van Kreveld, S., Andersson, C., Koç, N., Chapman, M., Sbaffi, L., Duplessy, J.-C., Sarnthein, M., Turon, J.-L., Duprat, J., Jansen, E., 2002. Apparent cooling of the sea surface in the northeast Atlantic and Mediterranean during the Holocene. *Quat. Sci. Rev.* 21, 455–483.
- Martrat, B., Grimalt, J.O., Villanueva, J., van Kreveld, S., Sarnthein, M., 2003. Climatic dependence of the organic matter contributions in the north-eastern Norwegian Sea over the last 15,000 years. *Org. Geochem.* 34, 1057–1070.
- März, C., Stratmann, A., Matthiessen, J., Meinhardt, A.-K., Eckert, S., Schnetger, B., Vogt, C., Stein, R., Brumsack, H.-J., 2011. Manganese-rich brown layers in Arctic Ocean sediments: composition, formation mechanisms, and diagenetic overprint. *Geochim. Cosmochim. Acta* 75, 7668–7687.
- Meyers, P.A., 1994. Preservation of elemental and isotopic source identification of sedimentary organic matter. *Chem. Geol.* 114, 289–302.
- Mugford, R., Dowdeswell, J.A., 2011. Modeling glacial meltwater plume dynamics and sedimentation in high-latitude fjords. *J. Geophys. Res.* 116, F01023.
- Mulder, T., Syvitski, J.P.M., Migeon, S., Faugères, J.-C., Savoye, B., 2003. Marine hyperpycnal flows: initiation, behaviour and related deposits. A review. *Mar. Pet. Geol.* 20, 861–882.
- Murdmåa, I., Ivanova, E., Duplessy, J.-C., Levitan, M., Khusid, T., Bourtman, M., Alekhina, G., Alekseeva, T., Belousov, M., Serova, V., 2006. Facies system of the Eastern Barents Sea since the last glaciation to present. *Mar. Geol.* 230, 275–303.
- Nieuwenhuize, J., Maas, Y.E.M., Middelburg, J.J., 1994. Rapid analysis of organic carbon and nitrogen in particulate materials. *Mar. Chem.* 45 (3), 217–224.
- Ottesen, D., Dowdeswell, J.A., Rise, S., 2006. Submarine landforms and the reconstruction of fast-flowing ice streams within a large Quaternary ice sheet: the 2500-km-long Norwegian–Svalbard margin (57°–80°N). *Geol. Soc. Am. Bull.* 117, 1033–1050.
- Pedrosa, M.T., Camerlenghi, A., De Mol, B., Urgeles, R., Rebesco, M., Lucchi, R.G., SVAIS and ECLACOM cruises shipboard parties, 2011. Seabed morphology and shallow sedimentary structure of the Storfjorden and Kveithola trough-mouth fans (north west Barents Sea). *Mar. Geol.* 286, 65–81.
- Peltier, W.R., 2005. On the hemispheric origins of meltwater pulse 1a. *Quat. Sci. Rev.* 24, 1655–1671.
- Petschick, R., Kuhn, G., Gingele, F., 1996. Clay mineral distribution in surface sediments of the South Atlantic: sources, transport, and relation to oceanography. *Mar. Geol.* 130, 203–229.
- Pfirman, S.L., Solheim, A., 1989. Subglacial meltwater discharge in the open-marine tide-water glacier environment: observations from Nordaustlandet, Svalbard Archipelago. *Mar. Geol.* 86, 265–281.
- Piper, D.J.W., Deptuck, M.E., Mosher, D.C., HughesClarke, J.E., Migeon, S., 2012. Erosional and depositional features of glacial meltwater discharges on the eastern Canadian continental margin. In: Prather, B.E., Deptuck, M.E., Mohrig, D.C., van Hoorn, B., Wynn, R.B. (Eds.), Application of Seismic Geomorphology Principles to Continental Slope and Base-of-slope Systems: Case Studies from Seafloor and Near-Seafloor Analogues. SEPM Special Publication, Tulsa, Society of Sedimentary Research, 99, pp. 61–80.
- Powell, R.D., 1990. Glacimarine processes at grounding-line fans and their growth to ice-contact deltas. In: Dowdeswell, J.A., Scourse, J.D. (Eds.), Glacimarine Environments: Processes and Sediments. Geological Society of London Special Publication, 53, pp. 53–73.
- Rasmussen, T.L., Thomsen, E., Slubowska, M.A., Jessen, S., Solheim, A., Koç, N., 2007. Paleooceanographic evolution of the SW Svalbard margin (76°N) since 20,000 14C yr BP. *Quat. Res.* 67, 100–114.
- Rebesco, M., Liu, Y., Camerlenghi, A., Winsborrow, M., Laberg, J.S., Caburlotto, A., Diviacco, P., Accettella, D., Sauli, C., Tomini, I., Wardell, N., 2011. Deglaciation of the Barents Sea Ice Sheet—a swath bathymetric and sub-bottom seismic study from the Kveithola Trough. *Mar. Geol.* 279, 141–147.
- Rebesco, M., Pedrosa, M.T., Camerlenghi, A., Lucchi, R.G., Sauli, C., De Mol, B., Madrussani, G., Urgeles, R., Rossi, G., Böhm, G., 2012. One million years of climatic generated landslide events on the northwestern Barents Sea continental margin. In: Yamada, Y., Kawamura, K., Ikehara, K., Ogawa, Y., Urgeles, R., Mosher, D., Chaytor, J., Strasser, M. (Eds.), Submarine Mass Movements and Their Consequences. Advances in Natural and Technological Hazards Research, Springer Science book series, 31, pp. 747–756.
- Rebesco, M., Wählin, A., Laberg, J.S., Schauer, U., Beszczynska-Möller, A., Lucchi, R.G., Noormets, R., Accettella, D., Zarayskaya, Y., Diviacco, P., 2013. Contourite drifts of the Western Spitsbergen margin. *Deep-Sea Res.* 179, 156–168.
- Reimer, P.J., Baillie, M.G.L., Bard, E., Bayliss, A., Beck, J.W., Blackwell, P.G., Bronk Ramsey, C., Buck, C.E., Burr, G.S., Edwards, R.L., Friedrich, M., Grootes, P.M., Guilderson, T.P., Hajdas, I., Heaton, T.J., Hogg, A.G., Hughen, K.A., Kaiser, K.F., Kromer, B., McCormac, F.G., Manning, S.W., Reimer, R.W., Richards, D.A., Southon, J.R., Talamo, S., Turney, C.S.M., van der Plicht, J., Weyhenmeyer, C.E., 2009. IntCal09 and Marine09 radiocarbon age calibration curves, 0–50,000 years cal BP. *Radiocarbon* 51, 1111–1150.
- Rinterknecht, V.R., Clark, P.U., Raisbeck, G.M., Yiou, F., Bitinas, A., Brook, E.J., Marks, L., Zelts, V., Lunkka, J.-P., Pavlovskaya, I.E., Piotrowski, J.A., Raukas, A., 2006. The Last Deglaciation of the Southeastern Sector of the Scandinavian Ice Sheet. *Science* 311, 1449.
- Rothwell, R.G., 1988. Minerals and Mineraloids in Marine Sediments. An Optical Identification Guide. Elsevier Science Publishers (279 pp.).
- Rüther, D.C., Mattingsdal, R., Andreassen, K., Forwick, M., Husum, K., 2011. Seismic architecture and sedimentology of a major grounding zone system deposited by the Bjørnøyrenna Ice Stream during Late Weichselian deglaciation. *Quat. Sci. Rev.* 30, 2776–2792.
- Rüther, D.C., Bjarnadóttir, L.R., Junttila, J., Husum, K., Rasmussen, T.L., Lucchi, R.G., Andreassen, K., 2012. Pattern and timing of the north-western Barents Sea Ice Sheet deglaciation and indications of episodic Holocene deposition. *Boreas* 41, 494–512.
- Sáez, A.G., Probert, I., Geisen, M., Quinn, P., Young, J.R., Medlin, L.K., 2003. Pseudo-cryptic speciation in coccolithophores. *Proc. Natl. Acad. Sci.* 100, 7163–7168.
- Sagnotti, L., Macri, P., Lucchi, R.G., Rebesco, M., Camerlenghi, A., 2011. A Holocene paleosecular variation record from the northwestern Barents Sea continental margin. *Geochem. Geophys. Geosyst.* 12 (11), Q11Z33.
- Sarkar, S., Berndt, C., Chabert, A., Masson, D.G., Minshull, T.A., Westbrook, G.K., 2011. Switching of a paleo-ice stream in northwest Svalbard. *Quat. Sci. Rev.* 30, 1710–1725.
- Sarnthein, M., 2011. Northern Meltwater Pulse, CO<sub>2</sub>, and changes in Atlantic convection. *Science* 331, 156–158.
- Shanmugam, G., 2000. 50 years of the turbidite paradigm (1950s–1990s): deep-water processes and facies models—a critical perspective. *Mar. Pet. Geol.* 17, 285–342.
- Shaw, J., Piper, D.J.W., Fader, G.B., King, E.L., Todd, B.J., Bell, T., Batterson, M.J., Liverman, D.J.E., 2006. A conceptual model of the deglaciation of Atlantic Canada. *Quat. Sci. Rev.* 25, 2055–2081.
- Shepherd, A., Wingham, D., Payne, T., Skvarca, P., 2003. Larsen Ice Shelf has progressively thinned. *Science* 302, 856–859.
- Sigmond, E.M.O., 1992. Bedrock map of Norway and adjacent ocean areas, scale 1:3 - million. Geological Survey of Norway.
- Skempton, A.W., 1954. Discussion of the structure of inorganic soils. *J. Soil Mech. Found. Div.* 80, 263–264.
- Skogseth, R., Hauganb, P.M., Jakobsson, M., 2005. Watermass transformations in Storfjorden. *Cont. Shelf Res.* 25, 667–695.
- Slubowska-Woldengen, M., Koç, N., Rasmussen, T.L., Klitgaard-Kristensen, D., Hald, M., Jennings, A.E., 2008. Time-slice reconstructions of ocean circulation changes on the continental shelf in the Nordic and Barents Seas during the last 16,000 cal yr B.P. *Quat. Sci. Rev.* 27, 1476–1492.
- Stanford, J.D., Rohling, E.J., Hunter, S.H., Roberts, A.P., Rasmussen, S.O., Bard, E., McManus, J., Fairbanks, R.G., 2006. Timing of meltwater pulse 1a and climate responses to meltwater injections. *Paleoceanography* 21 (4), PA4103.
- Stevens, R.L., 1990. Proximal and distal glacimarine deposits in southwestern Sweden: contrast in sedimentation. In: Dowdeswell, J.A., Scourse, J.D. (Eds.), Glacimarine Environments: Processes and Sediments. Geological Society of London Special Publication, 53, pp. 307–316.
- Stow, D.A.V., Holbrook, J.A., 1984. North Atlantic contourites: an overview. In: Stow, D.A.V., Piper, D.J.W. (Eds.), Fine Grained Sediments: Deep-Water Processes and Facies. Geological Society of London, Special Publication, 15, pp. 121–136.
- Stuiver, M., Reimer, P.J., 1993. Extended <sup>14</sup>C database and revised CALIB radiocarbon calibration program. *Radiocarbon* 35, 215–230.
- Svendsen, J.I., Alexanderson, H., Astakhov, V.I., Demidov, I., Dowdeswell, J.A., Funder, S., Gataulling, V., Henriksen, M., Hjort, C., Houmark-Nielsen, M., Hubberten, H.W., Ingólfsson, Ó., Jakobsson, M., Kjær, K.H., Larsen, E., Lokrantz, H., Lunkka, J.P., Lyså, A., Mangerud, J., Moutchkov, O., Murray, A., Möller, P., Niessen, F., Nikolskaya, O., Polyak, L., Saarnisto, M., Siegert, C., Siegert, M.J., Spielhagen, R.F., Stein, R., 2004. Late Quaternary ice sheet history of northern Eurasia. *Quat. Sci. Rev.* 23, 1229–1271.
- Syvitski, J.P.M., 1989. On the deposition of sediment within glacier influenced fjords: oceanographic controls. *Mar. Geol.* 85, 301–330.
- Taylor, J., Dowdeswell, J.A., Kenyon, N.H., Cofaigh, C.Ó., 2002. Late Quaternary architecture of trough-mouth fans: debris flows and suspended sediments on the Norwegian margin. In: Dowdeswell, J.A., Cofaigh, C.Ó. (Eds.), Glacially-Influenced Sedimentation on High-Latitude Continental Margins. Geological Society of London, Special Publications, 203, pp. 55–71.
- Teller, J.T., Leverington, D.W., Mann, J.D., 2002. Freshwater outburst to the oceans from glacial Lake Agassiz and their role in climate during the last deglaciation. *Quat. Sci. Rev.* 21, 879–887.
- Tomas, C.R., 1997. Identifying Marine Phytoplankton. Academic Press (858 pp.).

- Tripsanas, E.K., Piper, D.J.W., 2008. Late Quaternary stratigraphy and sedimentology of Orphan Basin: Implications for meltwater dispersal in the southern Labrador Sea. *Palaeogeogr. Palaeoclimatol. Palaeoecol.* 260, 521–539.
- Vogt, C., Knies, J., 2009. Sediment pathways in the western Barren Sea inferred from clay mineral assemblages in surface sediments. *Nor. J. Geol.* 89, 41–55.
- Vorren, T.O., Laberg, J.S., 1997. Trough mouth fans—palaeoclimate and ice-sheet monitors. *Quat. Sci. Rev.* 16, 865–881.
- Vorren, T.O., Plassen, L., 2002. Deglaciation and palaeoclimate of the Andfjorde Vagsfjord area, North Norway. *Boreas* 31, 97–125.
- Vorren, T.O., Hald, M., Thomsen, E., 1984. Quaternary sediments and environments on the continental shelf off northern Norway. *Mar. Geol.* 57, 229–257.
- Vorren, T.O., Lebesbye, E., Andreassen, K., Larsen, K.B., 1989. Glacigenic sediments on a passive continental margin exemplified by the Barents Sea. *Mar. Geol.* 85, 251–272.
- Vorren, T.O., Laberg, J.S., Blaume, F., Dowdeswell, J.A., Kenyon, N.H., Mienert, J., Rumohr, J., Werner, F., 1998. The Norwegian–Greenland sea continental margins: morphology and late quaternary sedimentary processes and environment. *Quat. Sci. Rev.* 17, 273–302.
- Wang, D., Hesse, R., 1996. Continental slope sedimentation adjacent to ice-margin II. Glaciomarine depositional facies on Labrador Slope and glacial cycles. *Mar. Geol.* 135, 65–96.
- Weaver, A.J., Saenko, O.A., Clark, P.U., Mitrovica, J.X., 2003. Meltwater pulse 1A from Antarctica as a Trigger of the Bølling–Allerød warm interval. *Science* 299, 709–1713.
- Weber, M.E., Clark, P.U., Ricken, W., Mitrovica, J.X., Hostetler, S.W., Kuhn, G., 2011. Inter-hemispheric ice-sheet synchronicity during the Last Glacial Maximum. *Science* 334, 1265–1269.
- Wetzel, A., Werner, F., Stow, D.A.V., 2008. Bioturbation and biogenic sedimentary structures in contourites. In: Rebesco, M., Camerlenghi, A. (Eds.), *Contourites*. Elsevier Developments in Sedimentology, 60, pp. 183–202.
- Winsborrow, M., Andreassen, K., Corner, G.D., Laberg, J.S., 2010. Deglaciation of a marine-based ice sheet: Late Weichselian palaeo-ice dynamics and retreat in the southern Barents Sea reconstructed from onshore and offshore glacial geomorphology. *Quat. Sci. Rev.* 29, 424–442.
- Wollenburg, J.E., Mackensen, A., 1998. Living benthic foraminifers from the central Arctic Ocean: faunal composition, standing stock and diversity. *Mar. Micropaleontol.* 34, 153–185.
- Young, J.R., 1998. Neogene. In: Bown, P.R. (Ed.), *Calcareous Nannofossil Biostratigraphy*. The Netherlands (Kluwer Academic Pub, Dordrecht, The Netherlands), pp. 225–265.
- Zajczkowski, M., 2008. Sediment supply and fluxes in glacial and outwash fjords, Kongsfjorden and Adventfjorden, Svalbard. *Pol.Polar Res.* 29, 59–72.
- Zwally, H.R., Abdalati, W., Herring, T., Larson, K., Saba, J., Steffen, K., 2002. Surface melt-induced acceleration of Greenland ice-sheet flow. *Science* 297, 218–222.